TU Delft

Bachelor Thesis

Reactor Instituut Delft

Passive emergency drainage of the Molten Salt Fast Reactor

Author:
Oliver van den Bergh

Supervisors:
Dr. Ir. Martin Rohde
Prof. Dr. Ir. Jan Leen Kloosterman

July 6, 2016

Abstract

Currently, R&D efforts are focussing on the development of the Generation IV Molten Salt Fast Reactor. The reference MSFR has a total fuel salt volume 18 m^3 and operates at a mean fuel temperature of 750 °C. The main safety measure of the MSFR is its fuel drainage system, enabling to drain the entire fuel salt volume to passively cooled underground tanks. During normal operation, the drainage pipe is closed by a actively cooled freeze plug which melts in case of a power outage. The resistance coefficients of the partially molten and completely molten freeze plug are respectively 2.59 and 0.19. Using these values, the drainage time for the reactor in combination with a 3.5 m drainage pipe is between 80 and 121 seconds, well below the prescribed 8 minutes after which damage occurs due to decay heat. Using a turbulent heat transfer model it is calculated that the hot fuel salt does not crystallize as it runs through the cold drainage pipe meaning no obstruction of the flow occurs.

List of Figures

Contents

Chapter 1

Introduction

Ever since the introduction of nuclear energy in the 1950's, nuclear safety has been a topic of great interest. Nuclear disasters such as the 1986 Chernobyl disaster and the 2011 Fukushima accident stress the importance of nuclear safety and the work to be done on it. Besides disasters, nuclear waste management is a topic that gained interest over the last several years. Traditional nuclear plants create waste that continues to be radioactive over tens of thousands of years. This means there is a great demand for safer, more efficient power plants that create less long-lived waste. Currently, the set of nuclear reactor that provide the required sustainability or increased efficiency are the Generation IV Reactors. In total there are six different kinds of reactors under research within the Generation IV framework: Very-high-temperature reactor (VHTR), Molten-salt reactor (MSR), Supercritical-water-cooled reactor (SCWR), Gas-cooled fast reactor (GFR), Sodium-cooled fast reactor (SFR) and the Lead-cooled fast reactor (LFR). The Reactor Instituut Delft (RID) is, among other involvements, heavily involved in research on the MSR. Together with 10 other partner universities, RID is part of the SAMOFAR- Safety Assessment of the Molten Salt Fast Reactor - project. This European project's goal is prove the innovative safety measures of the MSFR using advanced experiments and numerical methods. Extensive research is currently conducted in Delft and throughout Europe to prove this and to update the current conceptual design. This research focusses on design-related studies of the MSFR and in particular the drainage system in case of a station black out.

1.1 The MSFR in general

The standard MSFR is a 3000 MWth reactor with a total fuel salt volume of 18 m^3 (Heuer et al., 2014). The reactor operates at a mean temperature of about 750 °C. The core consists of cylinder in which the molten salt flows from the bottom to the top with no solid moderator present. The fuel returns to the bottom of the core through a system of 16 pumps and heat exchangers situated around the central core. This cycle takes 3-4 s to complete. The total amount of salt is equally split between the core and the heat exchangers, pumps etc. at all times. The cylindrical core has a height to diameter ratio approximately equal to one, this minimizes the neutron leaks and thus improves the breeding ratio. (Brovchenko et al., 2013) The system consists of the following elements (see figure 1.1) (EVOL, 2013):

- Core: The fuel salt enters the core at the bottom (the injection zone) with a temperature of approximately 650 °C. In the core itself, the actual nuclear fission takes place. This causes the temperature of the salt to rise 100 °C as it flows through the core. The higher temperature salt then leaves the core at the extraction zone at the top. The fuel salt's lower temperature limit is based on its melting point of approximately 565 °C since no solidification of the salt may occur throughout the system. The upper limit is based on the material constraints of the reactor. Operating temperatures above 750 °C can possibly damage the system.
- Fuel Salt: The optimal fuel salt composition is a binary fluoride salt composed of Lithium-Fluoride and a heavy nuclei composed of fertile thorium and fissile matter. The fission

products created during operation of the reactor, can be soluble or insoluble in the salt. In order to keep the operation running, the salt has to be cleaned in the process. Cleaning of the fuel salt happens through extraction of the fission products in the reprocessing unit.

- Upper and Lower Reflectors: The upper and lower walls of the core are made of a neutronic reflector. The material Hastelloy-N (a nickel alloy) seems to be most suited for this. Hastelloy-N can withstand great thermal stresses and is a good neutronic reflector. The upper reflector is subjected to higher thermal stresses due to the higher temperature.
- Fertile Blanket: The fertile blanket protects the external components of the fuels loops, including the pipes and heat exchangers. The walls of the blanket are made of the same materials as the reflectors. On this material a blanket of salt is situated with the same properties as the fuel salt but without any fissile material and a higher thorium concentration. The thorium is exposed to the core's neutron flux essentially making the fertile blanket a breeder of ^{233}U.
- Heat Exchangers: The 16 heat exchangers situated around the core prevent the core from overheating. Since the fuel salt heats up 100 °C inside the core, this heat has to be extracted in the system of heat exchangers. The extracted heat is then used to produce electricity.
- Pumps: In each of the external fuel loops, a pump is installed. Preliminary studies show that a fuel salt rate of $0.28\,m^3/s$ is enough for the right amount of fuel heating in the core and sufficient heat extraction in the heat exchangers.
- Reactor Vessel: The core and the external fuel loops are contained inside a reactor vessel. The vessel is build as an increased safety measure. The vessel is filled with the inert gas argon. The temperature of the argon gas is fixed at 400 °C, this has two functions: The gas cools down the hot reactor components and it allow for early detection of fuel salt leaks. Since the temperature of the gas is below the melting point of the fuel salt, possible leaking fuel will directly solidify.

In figure 1.1 the drainage system is not included. The drainage system is included to increase the safety of the reactor. The MSFR's safety measures are elaborated on in the next section.

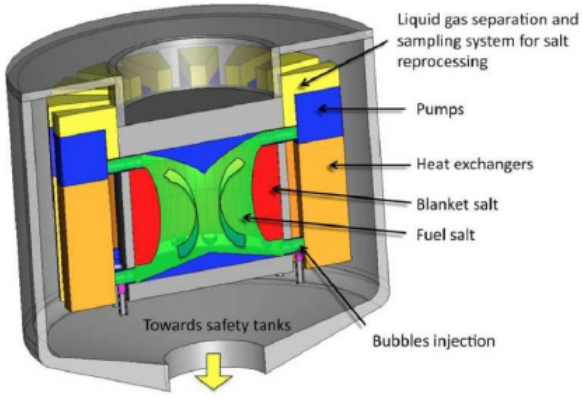

Figure 1.1: Conceptual design of the MSFR

1.2 Safety Assessment

In the new generation of nuclear reactors, safety is one of the key features to be considered. The MSFR is known for its elaborate safety features that ensure a reduced risk of accidents.

In figure 1.2 the entire reactor containment is depicted. The containment includes, in addition to the before described system, a fuel casing and storage spaces. The storage spaces are used as overflow tanks to compensate for any volume variations of the fuel salt due to temperature variations (Brovchenko et al., 2013). At the bottom of the core, a pipe leads the fuel into a, in a pool

submerged, fuel casing. This system is the MSFR's primary safety system. If, due to some kind of accident, the reactor loses electrical power the heat exchangers and pumps will fail. However, fission will continue in the core effectively increasing the fuel salt's temperature. A rise in temperature can damage the reactor vessel, if cracks occur in the vessel the fuel, including the radioactive material, can leak out. In order to prevent this a drainage system is installed. The drainage pipe is closed by a freeze plug: a plug made of solidified salt that is actively cooled. When power outage occurs, the freeze plug melts causing passive gravitational drainage of the fuel salt into the submerged fuel casing. In the fuel casing (or drainage tanks) the fuel salt is stored. In order to prevent overheating in the drainage tanks, the tanks are passively cooled. Moreover, the MSFR operates near atmospheric pressure greatly improving the safety compared to other pressurized reactors. This research will focus on the drainage time to completely drain the reactor and the design of the drainage pipe.

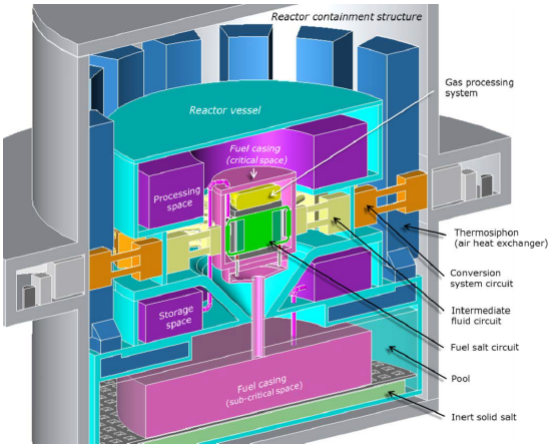

Figure 1.2: Conceptual design of the MSFR including drainage systems

1.3 Physicochemical properties

In order to correctly predict the heat transfer and flow rates, physicochemical properties of both the salt and the Hastelloy-N are required. The properties are summarized in the following tables:

Table 1.1: Physicochemical properties of the fuel salt (78% mol LiF - 22% mol Th_4). Based on EVOL (2013)

Property	**Formula**	**Value at** 700 °C	**Validity Range** °C
$\rho(\mathrm{g/cm^3})$	$4.094 - 8.82 \cdot 10^{-4}(T_k - 1008)$	4.1294	[620 - 850]
$\mu(\mathrm{Pa \cdot s})$	$\rho(\mathrm{g/cm^3}) \cdot 5.54 \cdot 10^{-5} e^{3689/T_k}$	$1.01 \cdot 10^{-2}$	[625 - 846]
$\lambda(\mathrm{W/m \cdot K})$	$0.928 + 8.397 \cdot 10^{-5} \cdot T_k$	1.0097	[618 - 747]
$C_p(\mathrm{J/kg \cdot K})$	$(-1.111 + 0.00278 \cdot T_k) \cdot 10^3$	1594	[594 - 634]

Table 1.2: Physicochemical properties of the Hastelloy-N

Property	**Formula**	**Validity Range** °C
$\rho(\mathrm{kg/m^3})$	$8932.719 - 0.2097391 \cdot T_k - 1.290039 \cdot 10^{-4} \cdot T_k^2$	[20 - 982]
$\lambda(\mathrm{W/m \cdot K})$	$0.4602577 + 0.0462231 \cdot T_k - 5.826548 \cdot 10^{-5} \cdot T_k^2 + 3.611111 \cdot 10^{-8} \cdot T_k^3$	[0 - 750]
$C_p(\mathrm{J/kg \cdot K})$	$254.5671 + 0.6849455 \cdot T_k - 7.911492 \cdot 10^{-4} \cdot T_k^2 + 3.651688 \cdot 10^{-7} \cdot T_k^3$	[20 - 540]
$C_p(\mathrm{J/kg \cdot K})$	$341112.4 - 1206.922 \cdot T_k^1 + 1.423109 \cot T^2 - 5.583335 \cdot 10^{-4} \cdot T_k^3$	[540 - 620]
$C_p(\mathrm{J/kg \cdot K})$	$682.8401 - 0.1085714 \cdot T_k$	[620 - 750]

The properties given in table 1.2 are based on the properties of Hastelloy-N in the Material Library of Comsol Multiphysics.

1.4 Goals and Outline

The goal of this research is to calculate the drainage time of the MSFR in emergency conditions. In order to do this, Computational Fluid Dynamics (CFD) is applied to compute the resistance coefficient of the freeze plug. Furthermore, CFD is combined with heat transfer into a non-isothermal turbulent flow theory to compute the temperature profile of the fuel salt in the drainage tube. The drainage tube is exposed to a pool (see figure 1.2) of water, heat transfer from the tube to the water is modelled in order to compute the temperature distribution in the flowing hot salt. From this temperature distribution one can investigate if any crystallization of the fuel salt takes place in the tubing. If so, this must be taken into account for the drainage time and drainage speed. The drainage time will be solved for analytically, turbulence modelling will be conducted in the multiphysics software Comsol.

In the next chapter, the background theory behind the drainage time, the resistance coefficient and the non-isothermal turbulence modelling is discussed in order to set up a framework that is used to solve the problem under research. In chapter 3 the software used, Comsol Multiphysics, will be elaborated on. Furthermore, the models used will be described including the applied boundary conditions and meshing requirements. Results of this research will be presented in chapter 4.

Chapter 2

Background Theory

2.1 Discharging tank problem

In order to ensure the safety of the reactor in case of a shut down the reactor has to be drained within 8 minutes. Otherwise, decay heat from the fissile fuel salt can overheat the system and damage the reactor, possibly resulting in a nuclear disaster (Brovchenko et al., 2013). To achieve this the drainage time of the reactor has to be calculated. This calculation is based on the 1D, steady-state mechanical-energy balance (van den Akker and Mudde, 1996):

$$0 = \phi_m \left(\frac{1}{2} v_1^2 + \frac{p_1}{\rho} + g z_1 - \frac{1}{2} v_2^2 - \frac{p_2}{\rho} - g z_2 \right) - \phi_m e_{diss} \tag{2.1}$$

In which ϕ_m is the mass flow through the exit pipe, v_i,p_i and z_i respectively the velocity, pressure and altitude at point i. Point 1 is set on the fuel level, point 2 at the outlet of the tank. The vessel which houses the molten salt is modelled as a $18\,\mathrm{m}^3$ cylindrical tank with a diameter to height ratio of 1. Initially, this tank is completely filled with the molten salt. Since the MSFR operates at atmospheric pressure the pressure difference between the salt level and the outlet is equal to zero ($p_1 = p_2$). Since the diameter of the drainage pipe is small in comparison to the reactor vessel's diameter, v_1 is negligible ($v_2 \gg v_1$). The temperature over the entire volume is taken constant and so is the density ρ. The height difference between the salt level and the outlet is denoted as $h(t) + L$, with $h(t)$ being the level in the actual tank and L the length of the attached drainage pipe. The energy dissipation e_{diss} is given by:

$$e_{diss} = \frac{1}{2} v^2 \left(4f \frac{L}{D} + K_{tot} \right) \tag{2.2}$$

In which f is the Fanning friction factor and D the diameter of the drainage pipe attached to the vessel. K_{tot} is the sum of all the resistance coefficients due to contractions, entrances, etc. For

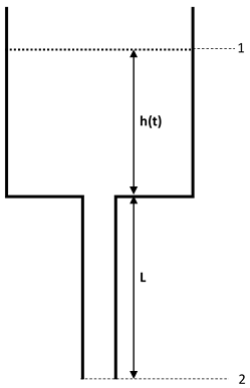

Figure 2.1: Cylindrical tank with a drainage pipe attached. The black dotted line is the fuel level.

specific values the reader is referred to Janssen and Warmoeskerken (1987). Note that the exit velocity v_2 is equal to velocity v since the diameter of the pipe is constant. Combining 2.1 and 2.2 results in the following expressing for the exit velocity:

$$\frac{1}{2}v_2^2(4f\frac{L}{D} + K_{tot}) = g(z_1 - z_2) - \frac{1}{2}v_2^2 \tag{2.3a}$$

$$v_2 = \sqrt{\frac{2g(h(t)+L)}{1+4f\frac{L}{D}+K_{tot}}} \tag{2.3b}$$

In order to solve for the time dependent salt level in the tank $h(t)$ the law of conservation of mass for this system is applied:

$$\frac{d}{dt}m_{tot} = \rho(v_1A_1 - v_2A_2) \tag{2.4}$$

Since v_1 is set to equal zero and m_{tot} can be denoted as $\pi\rho R_{tank}h(t)$ equations 2.3b and 2.4 can be rewritten to:

$$\frac{dh(t)}{dt} = -\frac{r^2}{R_{tank}^2}\sqrt{\frac{2g}{1+4f\frac{L}{D}+K_{tot}}}\sqrt{h(t)+L} = -k\sqrt{h(t)+L} \tag{2.5}$$

This equation yields a quasi-steady-state solution to the time dependence of the fluid level height in the reactor vessel:

$$h(t) = \frac{1}{4}(k^2t^2 - 2C_1kt + C_1^2 - 4L) \tag{2.6}$$

According to Bird et al. (1960) the change in total kinetic energy with time is negligible small and can thus be omitted, therefore the use of a steady-state mechanical energy balance is valid. A expression for the drainage time can be obtained by integrating equation 2.5 from $t = 0$ to $t = t_{drain}$ and $h = H_{tank}$ to $h = 0$. This results in:

$$t_{drain} = \frac{R_{tank}^2}{r^2}\sqrt{\frac{2\left(1+4f\frac{L}{D}+K_{tot}\right)}{g}}\left(\sqrt{H+L} - \sqrt{L}\right) \tag{2.7}$$

2.2 Turbulence Modelling

Turbulent pipe-flows are expected to occur in the draining duct. Previous studies on the drainage time predicts Reynolds numbers in the duct in the order of 10^5, resulting in a fully developed turbulent flow (Wang et al., 2016). Theoretical analysis of turbulence still is a fundamental problem in fluid dynamics. This is mostly due to the chaotic and unpredictable behaviour of turbulent flows. Fluid flows are governed by the Navier-Stokes continuity equations. Solving the Navier-Stokes equations for all length and time scales in a turbulent flow is computationally expensive and therefore nearly impossible. In order to solve for a turbulent flow, a different approach has to be considered. In the next section this research will elaborate on averaging the Navier-Stokes equations and solving the averaged Navier-Stokes equations using the k-ϵ and low-Reynolds k-ϵ models. (Celik, 1999)

2.2.1 Reynolds Averaged Navier-Stokes

For engineering applications, all turbulence models are based on the Reynolds Averaged Navier-Stokes equations. Instead of calculating all the time and length scales in a turbulent flow, the RANS model calculates mean velocities and pressures. In essence the RANS based turbulence models reflect a statistical viewpoint, as they do not compute detailed turbulence dynamics but the global effects of turbulence instead (Hulshoff, 2015). RANS is based of decomposing the flow in mean and fluctuating components:

$$u = \bar{u} + u' \tag{2.8}$$

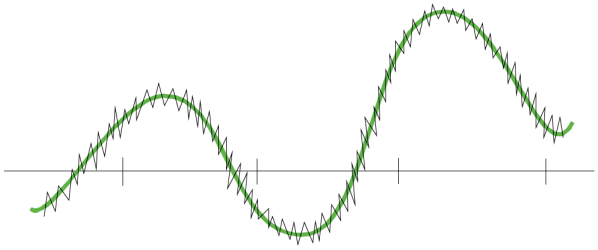

Figure 2.2: The concept of decomposing the velocity profile in a mean value (green line) and its fluctuating parts

The mean flow is a result of an ensemble average:

$$\bar{u}(x,t) = \lim_{N\to+\infty} \frac{1}{N} \sum_{N} u(x,t) \tag{2.9}$$

RANS equations are based on the incompressible Navier-Stokes Equations:

$$\frac{\partial u_i}{\partial x_i} = 0 \tag{2.10a}$$

$$\rho \frac{\partial u_i}{\partial t} + \rho u_j \frac{\partial u_i}{\partial x_j} = -\frac{\partial p}{\partial x_i} + \frac{\partial \tau_{ij}}{\partial x_j} \tag{2.10b}$$

where u_i is the velocity vector, p the pressure, ρ the density and τ_{ij} the viscous stress tensor defined by:

$$\tau_{ij} = 2\mu S_{ij} \tag{2.11}$$

in which μ is the molecular viscosity and S_{ij} is the strain-rate tensor defined by:

$$S_{ij} = \frac{1}{2}\left(\frac{\partial u_i}{\partial x_j} + \frac{\partial u_j}{\partial x_i}\right) \tag{2.12}$$

If equation 2.8 is substituted in the incompressible Navier-Stokes equations and time averaging the result the following is obtained (Hulshoff, 2015):

$$\frac{\partial \bar{u_i}}{\partial x_i} = 0 \tag{2.13a}$$

$$\rho \frac{\partial \bar{u_i}}{\partial t} + \rho \bar{u_j} \frac{\partial \bar{u_i}}{\partial x_j} = -\frac{\partial \bar{p}}{\partial x_i} + \frac{\partial}{\partial x_j}\left(\bar{\tau_{ij}} - \rho \overline{u_i' u_j'}\right) \tag{2.13b}$$

In comparison to equation 2.10 an extra term is introduced in the averaged equation above. This term, $-\rho\overline{u_i' u_j'}$ is referred to as the Reynolds stress tensor and couples the mean flow to the turbulence. The Reynolds stress is not a true stress in the conventional sense of the word. It actually represents the mean momentum fluxes induced by the turbulence. This new term is unknown and therefore needs to be modelled using a specific turbulence model. This is called the closure problem of turbulence. In this research modelling of the Reynols Stress is done using the k-ϵ and low Reynolds k-ϵ model.

2.2.2 Eddy Viscosity and Turbulent Kinetic Energy

Firstly, the concept of turbulent kinetic energy is introduced. The turbulent kinetic energy (TKE) is a measure for the kinetic energy per unit volume associated with the eddies in turbulent flows and defined as followed:

$$k = \frac{1}{2}\overline{u_i' u_i'} = \frac{1}{2}\left(\overline{u'^2} + \overline{v'^2} + \overline{w'^2}\right) \tag{2.14}$$

Using the TKE and a turbulent length scale, l, the kinematic eddy viscosity can be expressed as (Wilcox et al., 1998):

$$\nu_T = const. \cdot k^{\frac{1}{2}} l \tag{2.15}$$

The general idea behind the eddy viscosity is an analogy between the Reynolds stress and the laminar stress $\tau_{xy}^{laminar}$. Essentially the role of the turbulent viscosity is to ramp the overall viscosity from ν to $\nu + \nu_T$. The first step in determining k is taking the trace (sum of diagonal elements) of the Reynolds-stress:

$$\tau_{ii} = -\overline{u_i' u_i'} = -2k \tag{2.16}$$

Thus, the trace of the Reynolds-stress tensor is proportional to the kinetic energy of the turbulent fluctuations per unit volume. From this, a transport equation governing the turbulent kinetic energy can be derived (Wilcox et al., 1998):

$$\frac{\partial k}{\partial t} + \bar{u_j}\frac{\partial k}{\partial x_j} = \tau_{ij}\frac{\partial \bar{u_i}}{\partial x_j} - \epsilon + \frac{\partial}{\partial x_j}\left[\nu\frac{\partial k}{\partial x_j} - \frac{1}{2}\overline{u_i' u_i' u_j'} - \frac{1}{\rho}\overline{p' u_j'}\right] \tag{2.17}$$

The quantity ϵ is the dissipation per unit mass and is defined as:

$$\epsilon = \nu\overline{\frac{\partial u_i'}{\partial x_k}\frac{\partial u_i'}{\partial x_k}} \tag{2.18}$$

The Reynolds stress tensor in equation 2.17 is defined using the Boussinesq approximation (Wilcox et al., 1998) that results in the following:

$$\tau_{ij} = 2\nu_T S_{ij} - \frac{2}{3}k\delta_{ij} \tag{2.19}$$

The last two terms on the right-hand side of equation 2.17 are the turbulent transport and pressure diffusion respectively. The pressure diffusion term can be grouped with the turbulent transport term. The sum of these terms behave as a gradient-transport process. For simple flows this term is quite small thus the following can be assumed (Wilcox et al., 1998):

$$\frac{1}{2}\overline{u_i' u_i' u_j'} + \frac{1}{\rho}\overline{p' u_j'} = -\frac{\nu_T}{\sigma_k}\frac{\partial k}{\partial x_j} \tag{2.20}$$

In which σ_k is a closure coefficient. Combining equations 2.17 and 2.20 results in:

$$\frac{\partial k}{\partial t} + \bar{u_j}\frac{\partial k}{\partial x_j} = \tau_{ij}\frac{\partial \bar{u_i}}{\partial x_j} - \epsilon + \frac{\partial}{\partial x_j}\left[(\nu + \frac{\nu_T}{\sigma_k})\frac{\partial k}{\partial x_j}\right] \tag{2.21}$$

Equation 2.21 is the general turbulent kinetic energy that is used in all turbulence models. It is important to note that there are still parameters unknown, namely ϵ and l. Hence, a prescription for the length scale is needed to close the system of equations.

2.2.3 k-ϵ model

The k-ϵ model is a so called two-equation model. Two-equation models not only solve for k but also for the turbulent length scale. Therefore, all two-equation models are complete and can predict properties of a turbulent flow with no prior knowledge of the turbulence structure. In terms of the k-ϵ model the kinematic eddy viscosity and turbulent length scale are:

$$\nu_T \sim \frac{k^2}{\epsilon} \tag{2.22a}$$

$$l \sim \frac{k^{\frac{3}{2}}}{\epsilon} \tag{2.22b}$$

The general idea of the k-ϵ model is to define an exact equation for ϵ and to find closure approximations for the equation governing the behaviour of ϵ. This equation is given by:

$$\frac{\partial \epsilon}{\partial t} + \bar{u_j}\frac{\partial \epsilon}{\partial x_j} = C_{\epsilon 1}\frac{\epsilon}{k}\tau_{ij}\frac{\partial \bar{u_j}}{\partial x_j} - C_{\epsilon 2}\frac{\epsilon^2}{k} + \frac{\partial}{\partial x_j}\left[(\nu + \frac{\nu_T}{\sigma_\epsilon})\frac{\partial \epsilon}{\partial x_j}\right] \tag{2.23}$$

The turbulence kinetic energy equation is similar to 2.21. The kinematic eddy viscosity is equal to:

$$\nu_T = C_\mu\frac{k^2}{\epsilon} \tag{2.24}$$

The closure coefficients in the equations above are empirically determined by fitting the equations to common turbulent flows. The closure coefficients and the turbulence length scale are given by (Wilcox et al., 1998):

$$C_{\epsilon 1} = 1.44 \qquad C_{\epsilon 2} = 1.92 \qquad C_\mu = 0.09 \qquad \sigma_k = 1.0 \qquad \sigma_\epsilon = 1.3 \tag{2.25}$$

$$l = C_\mu \frac{k^{\frac{3}{2}}}{\epsilon} \tag{2.26}$$

2.2.4 Wall Functions

In wall bounded turbulent flows the turbulence pattern is not uniform. The turbulent flow near a flat wall can be divided up in four regions. At the wall, the fluid velocity is equal to zero (no slip condition). The first region is a thin layer above the wall in which the fluid velocity is linear with respect to the wall distance. This region is called the viscous sublayer or laminar sublayer. Some distance further away from the wall the buffer layer is situated, in this layer the transition to turbulent flow occurs. Eventually the buffer layer transitions to the log-law region. In this region the flow is fully turbulent and the average flow velocity is related to the logarithm of the wall distance. The final region is the free-stream flow region. The reader is referred to figure 2.3 for a schematic representation of the 4 regions (Frei, 2013).

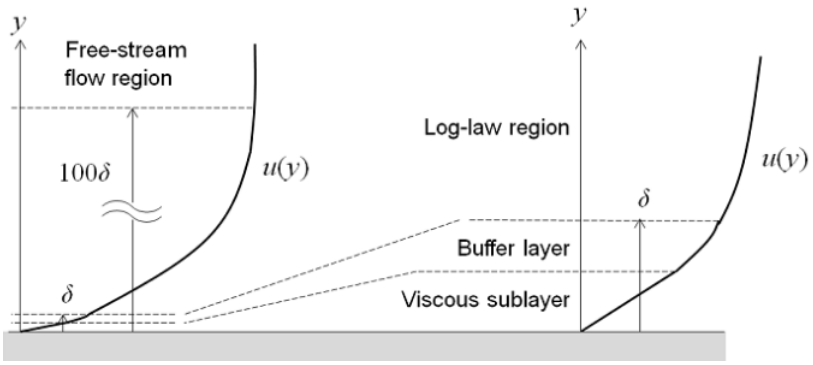

Figure 2.3: Schematic representation regions in wall bounded flow. Source: Frei (2013)

Solving the flow for all the regions is computationally expensive. This is where the wall functions are applied. Wall functions ignore the flow field in the buffer region and assume an analytic solution for the flow in the viscous layer. This means wall functions effectively lift the computational domain from the wall. As a consequence, turbulence is solved for in the free-stream and log-law region. Applying wall functions greatly reduces computational costs in comparison to models that solve the entire flow domain. Note that for some applications, such as near wall heat transfer, the turbulent flow for the entire domain has to be solved.

2.2.5 Low-Reynolds k-ϵ model

Since this research includes turbulent heat transfer the k-ϵ model is not predicted to be accurate enough. Heat transfer occurs near the wall, if wall functions are applied the heat transfer may be underestimated. This effect is due to near-wall eddies. Eddies transport energy much more efficient into the bulk of the flow compared to a laminar flow profile. The RANS model that solves the flow for the entire domain is called the Low-Reynolds k-ϵ model. Contradictory to what the name suggests, this model can be applied to high Reynolds number flows. This model is also based on the RANS equation 2.13. The equation that governs the turbulent kinetic energy is equal to the usual k-ϵ model, given by equation 2.21. The difference between this model and the usual model can be found in the energy dissipation and the eddy viscosity (Abe et al., 1994):

$$\frac{\partial \epsilon}{\partial t} + \bar{u_j}\frac{\partial \epsilon}{\partial x_j} = C_{\epsilon 1}\frac{\epsilon}{k}\tau_{ij}\frac{\partial \bar{u_j}}{\partial x_j} - C_{\epsilon 2} f_\epsilon \frac{\epsilon^2}{k} + \frac{\partial}{\partial x_j}\left[(\nu + \frac{\nu_T}{\sigma_\epsilon})\frac{\partial \epsilon}{\partial x_j}\right] \tag{2.27a}$$

$$\nu_T = C_\mu f_\mu \frac{k^2}{\epsilon} \tag{2.27b}$$

The difference compared to the usual model is tweaking of the constants with a function. The functions are given by:

$$f_\mu = \left(1 - e^{-\frac{l^*}{14}}\right)^2 \left[1 + \frac{5}{R_t^{0.75}} e^{-\frac{R_t}{200}^2}\right] \tag{2.28a}$$

$$f_\epsilon = \left(1 - e^{-\frac{l^*}{3.1}}\right)^2 \left[1 - 0.3e^{-\frac{R_t}{6.5}^2}\right] \tag{2.28b}$$

where

$$l^* = \frac{\rho u_\epsilon l_w}{\mu} \qquad R_t = \frac{\rho k^2}{\mu\epsilon} \qquad \mu_\epsilon = \frac{\mu\epsilon}{\rho}^{0.25} \tag{2.29}$$

With l_w being the distance to the closest wall. The closure coefficients are somewhat different compared to the usual model:

$$C_{\epsilon 1} = 1.5 \qquad C_{\epsilon 2} = 1.9 \qquad C_\mu = 0.09 \qquad \sigma_k = 1.4 \qquad \sigma_\epsilon = 1.4 \tag{2.30}$$

Note that this Two-Equation model requires more memory and computation time. Furthermore, an extra computational step is required to calculate l_w.

2.3 Turbulent Non-Isothermal Flow Theory

Turbulent non-isothermal flow theory combines heat and momentum transport in turbulent flows. In this research, this theory is required to solve the temperature distributions in the turbulent pipe flow in order to determine if any crystallization of the salt occurs in the system possibly blocking the flow.

2.3.1 The Temperature Equation

In order to research turbulent heat transfer a new density based average must be introduced, the Favre average:

$$\tilde{T} = \frac{\overline{\rho T}}{\bar{\rho}} \tag{2.31}$$

in which the bar denotes the usual Reynols average discussed in section 2.2.1. The temperature can then be denoted as the sum of the Favre average and the temperature fluctuations:

$$T = \tilde{T} + T' \tag{2.32}$$

Applying the Favre Average and Fourier's law for heat transfer $\left(q = -\lambda \frac{\partial T}{\partial x_j}\right)$ to the Navier-Stokes equation for the total internal energy in a flow results in the following equation that describes the temperature behaviour in a turbulent flow (COMSOL, 2015):

$$\bar{\rho} C_p \left(\frac{\partial \tilde{T}}{\partial t} + \tilde{u_j} \frac{\partial \tilde{T}}{\partial x_j}\right) = \frac{\partial}{\partial x_j}\left((\lambda + \lambda_T)\frac{\partial \tilde{T}}{\partial x_j}\right) + \tilde{\tau}_{ij}\tilde{S}_{ij} - \frac{\tilde{T}}{\tilde{\rho}}\frac{\partial \bar{\rho}}{\partial \tilde{T}}\left(\frac{\partial \bar{p}}{\partial t} + \tilde{u}_j \frac{\partial \bar{p}}{\partial x_j}\right) \tag{2.33}$$

Note that the Favre Average simplifies to the Reynolds average if the temperature dependence of the density is ignored. λ_T is the turbulent thermal conductivity which can be derived from the turbulent Prandtl number explained in section 2.3.2.

2.3.2 Turbulent Prandtl Number

Similar to the increment in viscosity by adding an eddy viscosity, the turbulent thermal conductivity in equation 2.33 increases the material's conductivity. However, the k-ϵ model does not solve for λ_T. This is where the turbulent Prandtl number comes in. The turbulent and effective thermal conductivity can be denoted as:

$$\lambda_T = \frac{C_p \mu_T}{Pr_T} \qquad \lambda_{eff} = \lambda_{material} + \lambda_T \tag{2.34}$$

In essence, the turbulent Prandtl number model describes the influence of turbulent fluctuations on the thermal conductivity. Thus, Pr_T describes the fraction to which the diffusivity of heat follows the diffusivity of momentum in a flow (Kays, 1994). The value for the turbulent Prandtl number is given by the following relation (Weigand et al., 1997):

$$Pr_T = \left(\frac{1}{2Pr_{T\infty}} + \frac{0.3}{\sqrt{Pr_{T\infty}}} \frac{C_p \mu_T}{\lambda} - \left(0.3 \frac{C_p \mu_T}{\lambda} \right)^2 \left(1 - e^{\frac{\lambda}{0.3 C_p \mu_T \sqrt{Pr_{T\infty}}}} \right) \right)^{-1} \tag{2.35}$$

In which $Pr_{T\infty}$ is equal to 0.85. C_p [J/(Kg K)] is the heat capacity at constant pressure and λ [W/(m K)] the thermal conductivity of the molten salt. Equation 2.35 is, according to Weigand et al. (1997), a good approximation for most kind of turbulent wall bounded flows such as pipe flows. μ_T is solved for in the k-ϵ model, this means that now a framework has been established to compute the temperature and velocity profile of turbulent flows.

2.4 Resistance Coefficient

In order to correctly predict the drainage time the exact value for K_{tot} in equation 2.3b has to be derived for the freeze plug's geometry. Calculation of the resistance coefficient is based on the mechanical-energy balance (eq. 2.1). This equation is now applied to the geometry of the freeze plug. The velocity throughout the plug is equal at the top and the bottom due to mass conservation in the tube, this means that $v_1 - v_2 = 0$. The geometry of the plug forces a difference in outlet and inlet pressure Δp which will be equated using CFD software. For this calculation the energy-dissipation is given by:

$$e_{diss} = \frac{1}{2} K v^2 \tag{2.36}$$

Combining equation 2.36 with 2.1 yields the following:

$$\frac{1}{2} K v^2 = \frac{1}{\rho}(p_1 - p_2) + g(z_1 - z_2), \qquad (v_1 = v_2) \tag{2.37a}$$

$$\frac{2\Delta p}{\rho} = K v^2 - 2g\Delta z \tag{2.37b}$$

Measuring the pressure difference between the inlet and outlet of the freeze plug for different values of flow velocity will result in a quadratic relation between pressure difference and velocity. From this relation the K value can be deduced. This K-value can then be used to calculate an accurate drainage time of the MSFR. Note that in this specific K-value the length of the plug's geometry is already included.

2.5 Heat Transfer in Solids

Heat transfer through the pipe wall from the hot salt to the surrounding of the tube must be modelled to achieve the desired level of accuracy. Heat transfer through any solid is based on the following equation:

$$\rho C_p \frac{\partial T}{\partial t} = \frac{\partial}{\partial x_i} \left(\lambda \frac{\partial T}{\partial x_i} \right) \tag{2.38}$$

In which C_p [J/(Kg K)] is the solid's heat capacity at constant pressure, ρ [kg/m^3] the solid's density and λ [W/(m K)] the solid's thermal conductivity. The heat is transported from the molten salt, through the wall, to the pipe surroundings. The pipe is surrounded by water, natural convection from the pipe wall to the water will govern the heat flux, this will be discussed with further detail in section 2.6. Equation 2.38 calculates the full time dependent temperature distribution in the wall, which can be used for further investigation of the thermal stress on the pipe walls.

2.6 Natural Convection

The heat sink for the hot molten salt will be the surrounding pool through which the piping runs. The process through which this occurs is natural convection. The fluid velocity field in the the pool is taken to be zero, this means that no forced convection occurs. Heat transfer will then occur predominantly through natural convection. The following equation holds for the convective heat flux:

$$q = h(T_{ext} - T_{wall}) \tag{2.39}$$

In which q [W/m^2] is the heat flux per unit area, h [W/(K $\cdot$ m^2)] the heat transfer coefficient and T_{ext} and T_{wall} are respectively the temperature of the wall and the temperature of the surroundings. In calculating the heat flux the heat transfer coefficient has to be known. Multiple relations exist for calculating the heat transfer coefficient for natural convection. In this research h is calculated using the following equation (Bergman et al., 2006):

$$h = \frac{\lambda}{L}\left(0.68 + \frac{0.67Ra_L^{1/4}}{\left(1+\left(\frac{0.492\lambda}{\mu C_p}\right)^{9/16}\right)^{4/9}}\right) \qquad (if\ Ra_L \leq 10^9) \tag{2.40a}$$

$$h = \frac{\lambda}{L}\left(0.825 + \frac{0.387Ra_L^{1/6}}{\left(1+\left(\frac{0.492\lambda}{\mu C_p}\right)^{9/16}\right)^{8/27}}\right)^2 \qquad (if\ Ra_L > 10^9) \tag{2.40b}$$

where L is the height of the tube and:

$$Ra_L = \frac{g\alpha_p\rho^2 C_p|T - T_{ext}|L^3}{\lambda\mu} \tag{2.41}$$

where g [m/s^2] is the gravitational acceleration and α_p[1/K] is the coefficient of thermal expansion of the surrounding fluid. All material properties in the equations above are of the surrounding fluid in which the natural convection occurs and are evaluated at $(T+T_{ext}/2)$. Ra_L is the Rayleigh number, the product of the Grashof and Prandtl number. The Rayleigh number indicates through which process heat transfer occurs, conduction of convection. High Rayleigh numbers indicate that heat transfer predominantly occurs through convection.

In sections 2.1 through 2.6 a general framework has been established to calculate the drainage time of the reactor's fuel salt and the temperature profile in the tubing. Using the calculated resistance coefficient an accurate drainage time can be calculated. From this drainage time a time dependent velocity through the pipes can be deducted. Using this velocity as an inlet input the temperature profile can be calculated using turbulence modelling for momentum and temperature. Modelling this process will be done numerically using the Comsol software which will be discussed in the next chapter.

Chapter 3

Numerical Methods

3.1 COMSOL

The set of equations introduced in chapter 2 are solved using Comsol Multiphysics. Comsol can be used to solve a variety of physics related problems such as the problem proposed in this research. The primary advantage of using Comsol is that no in-depth knowledge of numerical analysis is required. Besides calculating, Comsol is a great tool for analysis of the output data, no secondary software is required. The geometries under research can be build within the GUI, after which a particular physics interface has to be added containing the set of equations. Boundary conditions related to this physics interface are defined by the user over the domains and boundaries of the particular geometry. Comsol then solves the physics using the finite element method. Comsol solves both stationary and time-dependent studies. In this research Comsol is used to compute the turbulent flow and heat transfer, drainage times are computed analytically using Matlab.

3.2 Model 1: Resistance Coefficient

In this section the Comsol application for determining the resistance coefficient of the freeze plug is explained.

3.2.1 Geometries

The resistance coefficient for the freeze plug will be researched in two conditions: closed and open (both based on a design by Koks (2016)). The closed plug is depicted in figure 3.1. In this scenario, the upper part of the plug has melted in such a way that the molten salt can run freely along the frozen salt plug. Note that the plug is completely solidified, the flow is obstructed by a block of frozen salt. In the second situation, the entire plug has melted and is completely opened. In this situation nearly no obstruction of the plug should occur, only the cooling elements are still present in the flow. The general idea is that as the upper part of the plug melts the hot salt can run freely along the plug (closed plug situation). Forced convection will then cause the entire plug to melt or slide out of position as the friction between the solid salt and the cooling elements lessens due to a thin melted layer of salt. After the plug slides out the flow is not obstructed any more causing quick drainage of the reactor (open plug situation).

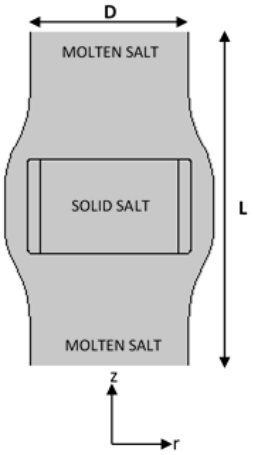

Figure 3.1: Closed Plug

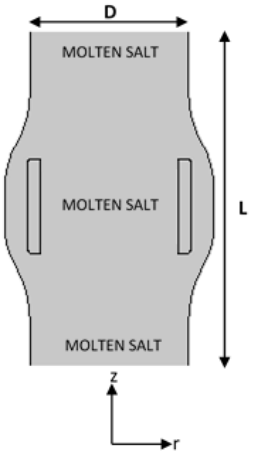

Figure 3.2: Open Plug

D is the diameter of the drainage pipe, taken to be 20 cm (Wang et al., 2016). L is the distance between the measuring points of the pressure p_i. The positions for measuring p_i are further elaborated on in section 4.1. In the true Comsol application, the computational domain has a total length of 2.15 m (inlet to outlet) for both models. In comparison, the length of the plug depicted in figures 3.1 and 3.2 is approximately 0.5 m. This longer domain is required to correctly introduce turbulence modelling, a too short domain imposes boundary conditions in developing flow resulting in incorrect measurements. Furthermore, the application uses symmetry to increase calculation speed. The symmetry axis is located at $r = \frac{1}{2}D$, the 3D images generated are revolved around this axis.

3.2.2 Boundary Conditions and Meshing

Preliminary results of the drainage time showed that Reynolds numbers in the flow will be in the turbulent regime. Therefore, the Comsol physics interface used is the Turbulent Flow, k-ϵ interface. Involving the physics for this interface is done through adding boundary conditions to the geometry:

- Inlet: The same inlet boundary condition is applied on both plugs. The inlet is defined at the top boundary of the geometry and defines a inlet velocity in the negative z direction. The inlet velocity ranges from -2 to -6.5 m/s in steps of 0.5 m/s.
- Outlet: On both plugs, the same outlet condition is applied. The outlet is defined on the lowest boundary of the geometry. On this boundary atmospheric pressure is applied: p_2=1 atm. Furthermore, backflow is supressed, this option adjusts the outlet pressure in order prevent fluid from re-entering the domain through the boundary. Moreover, normal flow is applied, this forces the flow to exit the pipe perpendicular to the outlet.
- Walls: The first wall is defined at the outer left and right boundaries, included the curved features around the actual plug. In the closed plug, the upper and lower boundary of the frozen salt are also defined as a wall. Furthermore, the part of the cooling element in contact with the fluid is defined as a wall boundary. In the open plug, since no frozen salt is present, the entire circumference of the cooling element is defines as a wall boundary. Is essence, every boundary in contact with the molten salt is defined as a wall apart from the inlet and outlet. At the wall boundaries, wall functions are applied (equivalent to the no slip condition for laminar flow).
- Initial Values: At the inlet, the turbulent kinetic energy [m^2/s^2] and the turbulent dissipation rate [m^2/s^3] both have the standard Comsol value of 0.005. Note that this only applies for the lowest velocity, studies at higher inlet velocities use the values generated by the previous study as new initial values.

The problem is solved with a stationary solver with an auxiliary sweep for the 10 different inlet velocities. This means the software solves and saves the data for each inlet velocity and uses the results of the previously solved inlet velocity as initial values for a higher velocity, this greatly increases computational speed. Furthermore, an 'average' function is defined on the boundary at which the pressure is measured. This average function computes the average of any given variable over that specific boundary, in this section it will only be used to calculate the average pressure.

The quality of the mesh is of great importance to retrieve accurate results. A balance has to be found between accuracy and computation time. The mesh is split up in 3 parts:

1. The inflow domain (0.7 m of pipe placed above the geometries in figures 3.1 and 3.2): Physics Controlled Fluid Dynamics Mesh set to 'Finer'.
2. The middle domain: location of the actual plug with a Physics Controlled Fluid Dynamics Mesh set to 'Extra Fine'.
3. The outflow domain (0.9 m of pipe place below the middle domain):Physics Controlled Fluid Dynamics Mesh set to 'Finer'.

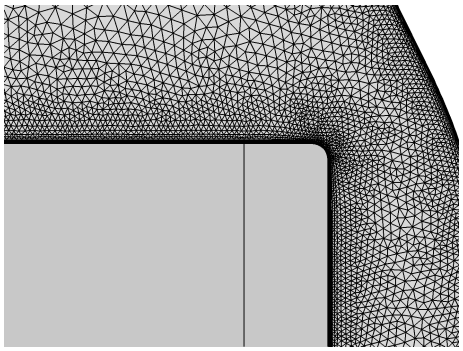

Figure 3.3: Closed Plug Mesh

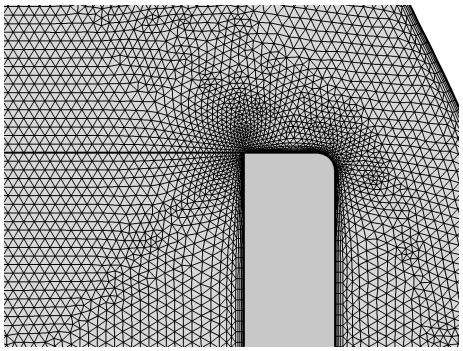

Figure 3.4: Open Plug Mesh

With these mesh settings the computational time taken for both plugs was just under 6 hours. A close-up of both meshes is depicted in figures 3.3 and 3.4. The mesh is very fine near the walls, this corresponds to the places where the largest gradients and smallest flow scales are expected.

In order to check the accuracy of the turbulent flow calculations the value of the wall lift-off in viscous units has to checked. The wall lift-off in viscous units is calculated using (COMSOL, 2015):

$$\delta_w^+ = \frac{\rho C_\mu^{0.25} \sqrt{k} \delta_w}{\mu} \tag{3.1}$$

δ_w is the distance at which the computational domain is located if wall functions are applied. δ_w^+ corresponds to the distance from the wall where the logarithmic layer meets the viscous sublayer. The value for δ_w^+ should be equal to 11.06 for the highest accuracy. However, high accuracy is also achieved if this value is slightly higher at some parts of the wall (COMSOL, 2015).

3.3 Analytical Drainage Time and Velocity

Equation 2.5 can be solved by introducing the following boundary condition: $h(0) = H_{tank}$. This corresponds to a fuel level equal to the tank height before drainage starts, in essence a completely filled reactor. Applying this condition to equation 2.5 leads to an expression for the fuel height in the tank:

$$h(t) = \frac{k^2}{4} t^2 - \sqrt{H + L} \cdot kt + H \tag{3.2a}$$

$$k = \frac{r^2}{R_{tank}^2}\sqrt{\frac{2g}{1 + 4f\frac{L}{D} + K_{tot}}} \tag{3.2b}$$

The results presented in chapter 4 are produced using Matlab. Equation 3.2 is inserted in a Matlab script and solved for with varying K_{tot} values. Using the solution of equation 3.2 as an input for the height in equation 2.3b results in a solution for the fluid flow velocity in the drainage pipe. This data is also analysed using Matlab. Moreover, Matlab is used to calculate resistance coefficients of the plug from the pressure data generated by Comsol. Equation 2.37b is the fundamental equation in this Matlab script. Estimation of the resistance coefficient is done by plotting a 1st order polynomial to the pressure data and applying the least squares method to generate the best fit.

3.4 Model 2: Pipe Flow Temperature Distribution

In this section the application used for determining the temperature distribution in the drainage pipe is discussed. This model solves the equations presented in sections 2.2 through 2.6.

3.4.1 Geometry

In order to achieve accurate results within a reasonable amount of time the full 3.5 metres of pipe is not completely modelled. Instead, the first 1.5 metres are regarded as insulated, since this part runs through the thick lower reflector. Only the part of the pipe in contact with the pool is modelled since most of the heat exchange, an thus cooling of the salt, is expected in this domain. The diameter and length of the pipe are 0.2 and 2 m respectively. The pipe wall is made of a 1 cm thick layer of Hastelloy-N (Merle-Lucotte et al., 2014). Figure 3.5 depicts a sketch of the system. The full length of the pipe is exposed to the water. The pipe is modelled in 2D applying symmetry by defining a symmetry axis (red dotted line). The application solves for half of the domain and mirrors its outcomes on the symmetry axis.

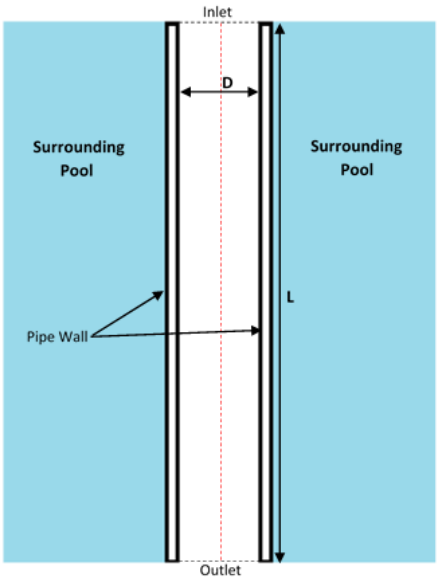

Figure 3.5: Second part of the drainage pipe running through the pool below the reactor core, not on scale

3.4.2 Boundary Conditions and Meshing

The physics interfaces applied to this model are the Low-Reynolds k-ϵ Turbulent Flow and the Heat Transfer in Fluids interfaces. These components are combined using the Non-Isothermal Flow Coupling interface. The model is solved using a time-dependent study since the inlet velocity is time dependent. The following boundary conditions and initial values are applied to the model:

- Inlet: At the inlet a time dependent inlet velocity is defined. This function, $v(t)$, is a result of the drainage velocity calculations presented in section 4.2. In general, CFD programs have difficulty with initializing the calculation if the initial value for the velocity is high. Because of this reason a smooth step function is applied to the inlet velocity. This step function is defined in such a way that it ramps the velocity from 0 to $v(0)$ m/s in 1 second (see figure 3.6). From there on $v(t)$ governs the inlet velocity. The inlet is defined at the upper horizontal boundary of the model (see figure 3.5).
- Outlet: The same conditions as in the resistance coefficient application are applied (see 3.2.2).
- Wall: The side of the wall exposed to the molten salt is set to the no slip boundary condition.
- Fluid Properties & Initial Values: The fluid properties are defined by the formulas in table 1.1. However, since λ and μ hardly change with temperature they are taken to be constant for a value of 750 °C in order to decrease computational time. The initial value for the turbulent kinetic energy en dissipation rate are the Comsol default values.
- Heat transfer in solids: Within the heat transfer in fluids interface the wall is set to a heat transfer in solids domain in order to model heat conduction through the Hastelloy-N wall.
- Temperature Boundary: At the inlet the temperature is set to 750 °C, the temperature at which the MSFR nominally runs. Discontinuous Galerkin constraints are applied to this boundary since this does not force temperature at the wall to be 750 °C.
- Outflow: At the outlet the heat boundary condition applied is outflow. This condition states that the only transfer occurring across the boundary is by convection.
- Heat Flux: At the outer wall, in contact with the pool, a convective heat flux along the entire length of the pipe is applied. The heat flux is modelled using equation 2.40. The temperature of the surrounding pool is set at 20 °C.
- Thermal Insulation: The upper and lower horizontal boundaries of the wall are thermally insulated. This means there is no heat flux across the boundary.
- Initial Values: Two initial values domains are added for the heat transfer interface. The initial temperature of flow domain (domain within the walls) is set to 750 °C. This is physically not correct since at $t = 0$ this domain would be the same temperature as its surroundings. However, this saves a lot of computational time since the software does not have to solve the propagation of the heat front through the domain. Since at a velocity of 6 m/s the salt flows through the pipe in 0.3 seconds, this is a valid assumption. The initial values of the wall are set to 20 °C.
- Non-Isothermal Flow Coupling: Coupling of the heat transfer and turbulent flow interface occurs through Kays-Crawford model for the Turbulent Prandtl number (see section 2.3.2).

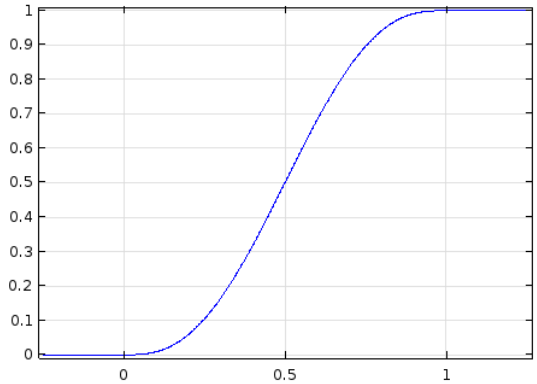

Figure 3.6: Step function applied to the time dependent inlet velocity in order to improve convergence. The x-axis displays time and the y-axis the factor to which it ramps $v(0)$.

As mentioned before, this model is solved using a time dependent solver consisting of two steps:

1. Wall Distance Initialization: This step solves for the distance to the closest wall: l_w (see 2.2.5).

2. Time Dependent: The following settings are applied for the time stepping: [range(0,0.5,3) range(4,2,80)]. 80 seconds is equal to the time to drain the reactor, further elaborated on in the results. At these time steps the results are saved, so they can be plotted in the result section. The actual solver takes much smaller internal steps.

As for the previous model, correct meshing is vital for retrieving accurate results. In contradiction to the previous model the mesh applied on this model is user defined. The physics defined mesh by Comsol is triangular by default, since this model is perfectly rectangular a rectangular mapped mesh suits this model better, it allows for more accurate results with fewer elements.

For the Low-Re k-ϵ model the dimensionless distance to cell centre, l_c^*, is parameter to check in order to conclude that the mesh is accurate enough. l_c^* is the distance, measured in viscous units, from the wall to the centre of the wall's adjacent cell. Ideally, the value for l_c^* is below 0.5. A mesh refinement study is conducted in all the Comsol models to monitor the influence of varying the mesh size. Results for the most accurate meshes are presented in this research. Calculations took just under 9 hours with the meshes depicted in the figures below.

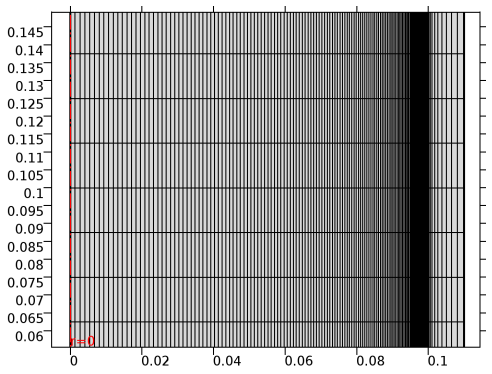

Figure 3.7: Mesh over entire width of the pipe with the symmetry axis coloured red (at r=0).

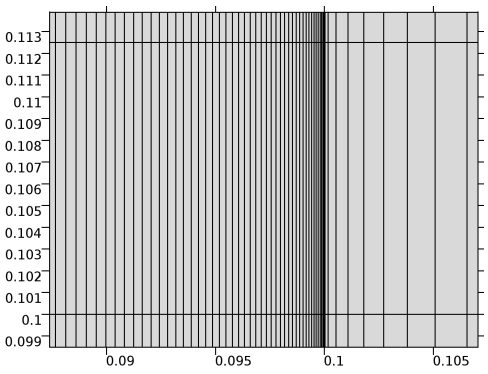

Figure 3.8: Close up of the near wall mesh. The wall starts at r=0.1.

Chapter 4

Results

In this chapter the results for the CFD calculations on the resistance coefficient of the plug, the drainage time of the tank and the CFD calculations on the temperature profile in the drainage pipe will be presented.

4.1 Resistance Coefficient

In this section the results of the resistance coefficient calculation of the open and closed plug are presented. As mentioned previously, both coefficients are calculated using k-ϵ turbulence modelling in combination with the mechanical-energy balance.

4.1.1 Closed Plug

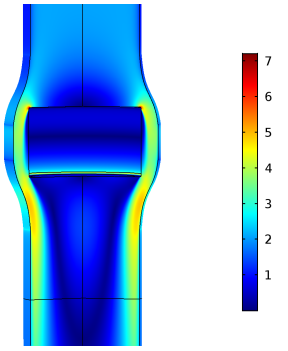

Figure 4.1: Velocity magnitude $|\vec{u}|$ throughout the closed plug with an inlet velocity of 2 m/s

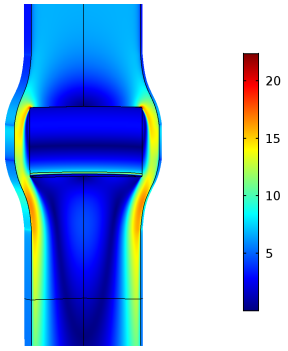

Figure 4.2: Velocity magnitude $|\vec{u}|$ throughout the closed plug with an inlet velocity of 6.5 m/s

A 2D graphic result of the application is depicted in figures 4.1 and 4.2. For other inlet velocities, this figure look similar; only the lowest and highest inlet velocities are depicted. In order to retrieve an accurate resistance coefficient, research is done into the velocity profile in the outlet domain. The outlet domain extends 1.1 m from the bottom of the solid ice to the actual outlet boundary. The velocity profile for different distances from the outlet boundary is given in figure 4.3. For different inlet velocities, the graph look very similar.

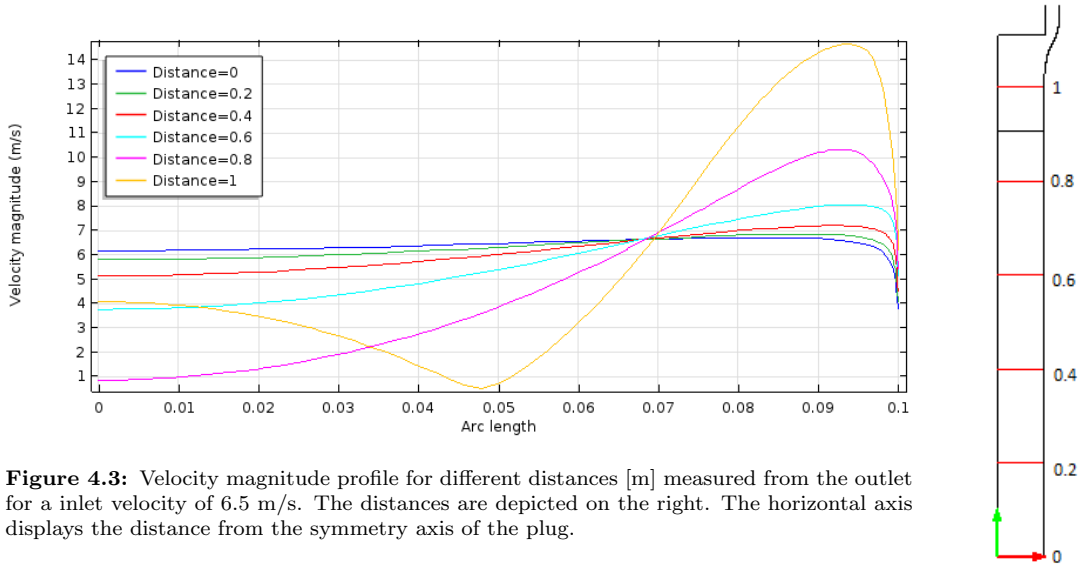

Figure 4.3: Velocity magnitude profile for different distances [m] measured from the outlet for a inlet velocity of 6.5 m/s. The distances are depicted on the right. The horizontal axis displays the distance from the symmetry axis of the plug.

For the inlet's domain velocity profiles a similar analysis has been conducted:

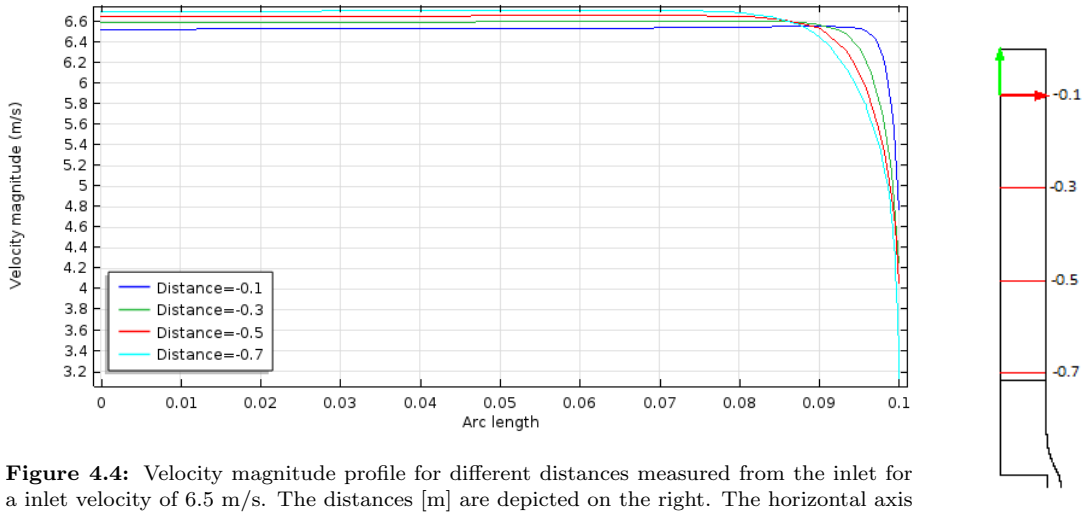

Figure 4.4: Velocity magnitude profile for different distances measured from the inlet for a inlet velocity of 6.5 m/s. The distances [m] are depicted on the right. The horizontal axis displays the distance from the symmetry axis of the plug.

From figure 4.3 one can deduce that as the flow approaches the outlet the velocity profile straightens out. For this reason p_2 is measured at the outlet boundary. The velocity profile in the inlet domain is depicted in figure 4.4. Clearly, the flow develops as is moves down the pipe but the overall velocity profile is flat. For simplicity reasons, p_1 is measured just above the plug at the black coloured horizontal boundary depicted in the right figure of 4.4. This makes the overall distance, Δz, between p_1 and p_2 1.435 m. Based on equation 2.37b the pressure difference correct by the density ($\frac{p_1 - p_2}{\rho}$) is plotted against the different inlet velocities:

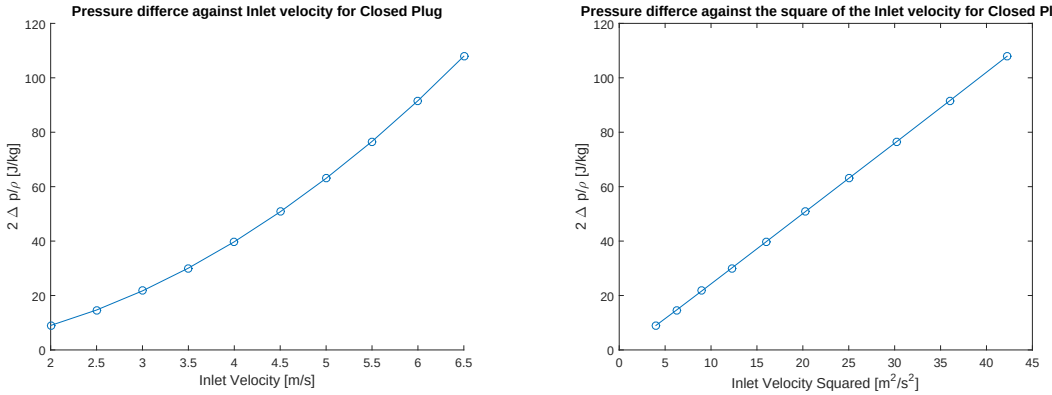

Figure 4.5: Pressure difference between two measuring boundaries of the plug as a function of inlet velocity and the square of the inlet velocity. $\rho = 4125\,\mathrm{kg/m^3}$

As expected Δp is proportional to the square of the inlet velocity. To further confirm this, Δp is plotted against the square of the velocity, this time showing a linear proportionality. This confirms our expectations presented in section 2.4. In figure 4.5, the K value represents the slope of the right graph. The slope is determined using MATLAB's 1 degree polyfit function, which applies the least-squares method. This results in $K_{closed} = 2.59$.

4.1.2 Open Plug

Calculations of the resistance coefficient of the open plug are analogous to the previous section.

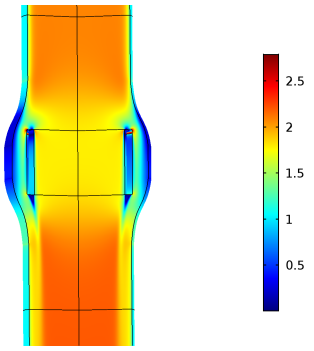

Figure 4.6: Velocity magnitude $|\,\vec{u}\,|$ throughout the open plug with an inlet velocity of 2 m/s

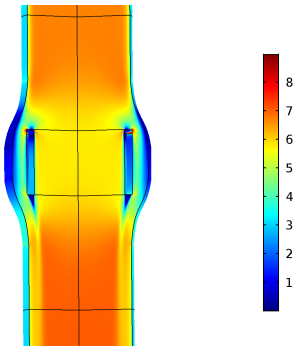

Figure 4.7: Velocity magnitude $|\,\vec{u}\,|$ throughout the open plug with an inlet velocity of 6.5 m/s

As expected, the flow is much less obstructed in comparison the the closed plug situation. Moreover, the velocity fluctuations throughout the flow are much smaller. In the outlet domain, the velocity profile is measured on the same boundaries as in 4.3 resulting in:

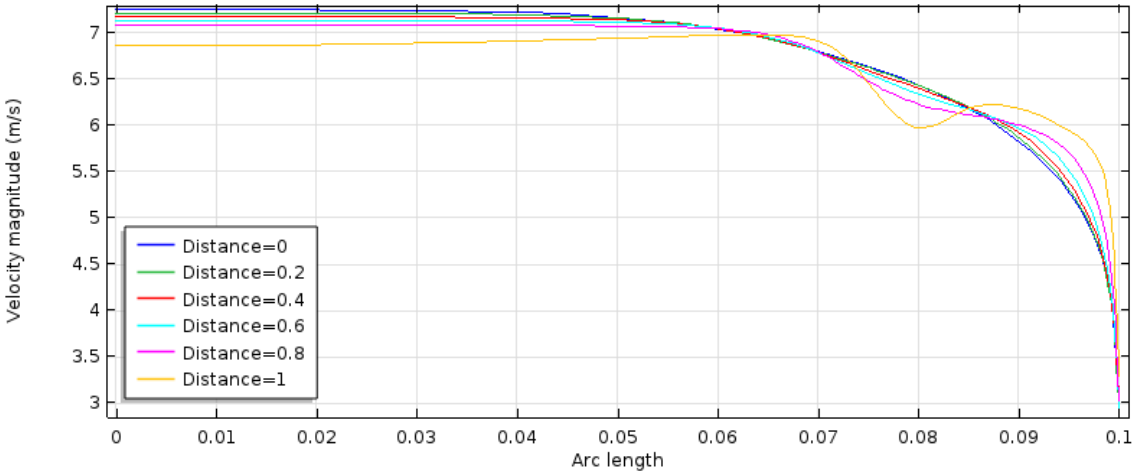

Figure 4.8: Velocity magnitude profile for different distances measured from the outlet for a inlet velocity of 6.5 m/s. The horizontal axis displays the distance from the symmetry axis of the plug. All distances are in [m].

Figure 4.8 confirms that the open plug hardly interferes the flow profile. The velocity profile straightens out much quicker, due to the smaller fluctuations, than it does with the closed plug. The velocity profile at the inlet domain is similar to the graph depicted in 4.4. In order to compare the results, pressure measurements are conducted at the same positions as for the closed plug.

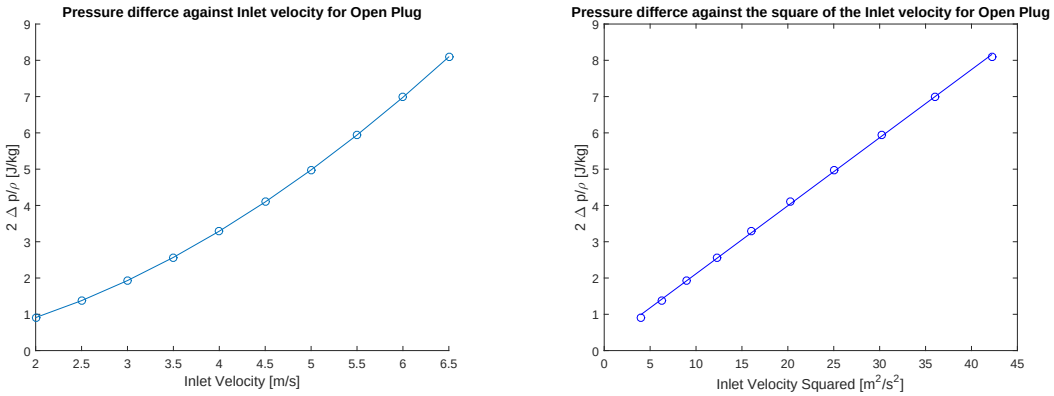

Figure 4.9: Pressure difference between two measuring boundaries of the plug as a function of inlet velocity and the square of the inlet velocity. $\rho = 4125\,\mathrm{kg/m^3}$

Figure 4.9 displays similar results compared to figure 4.5. However, the pressure differences are much smaller. This confirm our suspicion that melting of the frozen salt results in a much lower resistance coefficient. A 1st degree polyfit to the linear graph on the right results in $K_{closed} = 0.19$.

As expected, the closed plug imposes greater resistance on the flow compared to the open plug. The influence of the plugs on the drainage time of the molten salt reactor will be researched in the next section.

4.2 Drainage Time

4.2.1 Fanning Friction Factor

The Fanning friction factor (f) is calculated for smooth pipes since no wall roughness is taken in account in calculating the resistance coefficient of the plugs in Comsol. Besides, the roughness height for Hastelloy-N is not well documented. For these reasons, f is calculated using (Morrison,

2013):

$$f = \frac{16}{Re} + \left(\frac{0.0076 \left(\frac{3170}{Re} \right)^{0.165}}{1 + \left(\frac{3170}{Re} \right)^{7}} \right) \qquad Re < 10^6 \tag{4.1a}$$

$$Re = \frac{\rho v D}{\mu} \tag{4.1b}$$

According to Wang et al. (2016), the drainage velocity in the tube will differ from approximately 4.5 to 7 m/s, for these values Reynolds is well below 10^6 so equation 4.1, together with the values given in table 4.1, holds:

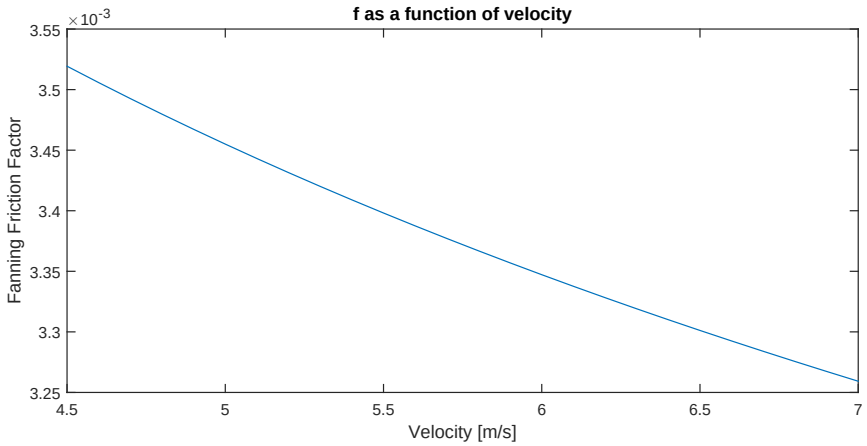

Figure 4.10: Fanning friction factor as a function of pipe flow velocity

From figure 4.10 it can be deduced that f is very small and fairly constant. For this reason, f is taken to be a constant. Without this simplification equation 2.5 cannot be solved analytically since f would be velocity dependent. Taking the mean from figure 4.10 result is a value for f of 0.0034.

4.2.2 K_{tot} dependency of drainage time

In this section, the results of the resistance coefficient's influence on the drainage time of the MSFR are presented. The figures presented are based on the equations elaborated on in section 2.1 together with the resistance coefficients calculated in section 4.1. The following parameters are applied:

Table 4.1: Constants applied in calculating the drainage time and velocity

R_{tank}[m]	H_{tank} [m]	r_{pipe} [m]	ρ [kg/m^3]	f	K_{inlet}
1.42	2.84	0.1	4125	0.0034	0.5

This study investigates 3 drainage situations:

1. No obstruction of the pipe
2. Open (molten) freeze plug
3. Closed (partially molten) freeze plug

Since the length of the plug equals 1.435 m (including in- and outflow domain) the total length of the exit pipe is the sum of the plug length and the additional pipe length. Estimated is that 3.5 meters is a reasonable total pipe length to reach sufficiently below the core to safely store the molten salt. Therefore, the additional pipe lengths equals 2.065 meter. This means that in

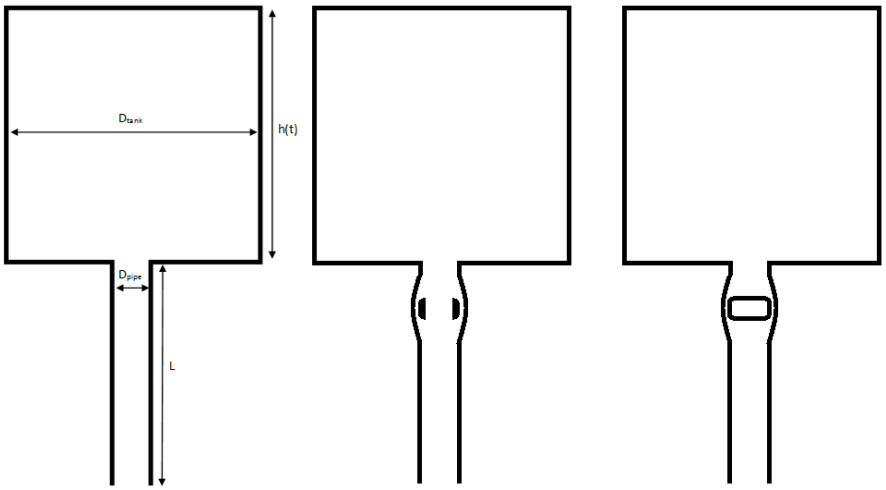

Figure 4.11: No obstruction, Open Plug and Closed Plug respectively

situation 1 L in equation 2.5 is the same for the $4f\frac{L}{D}$ (term due to friction) and the $\sqrt{L+h(t)}$ (term due to pressure drop) term. For situation 2 and 3 the L in $4f\frac{L}{D}$ is only 2.065 meter where the L in $\sqrt{L+h(t)}$ equals 3.5 meter (because friction is included in the K-value of the plug). Introducing equation 2.6 with boundary condition $h(0) = H_{tank}$ in MATLAB results in:

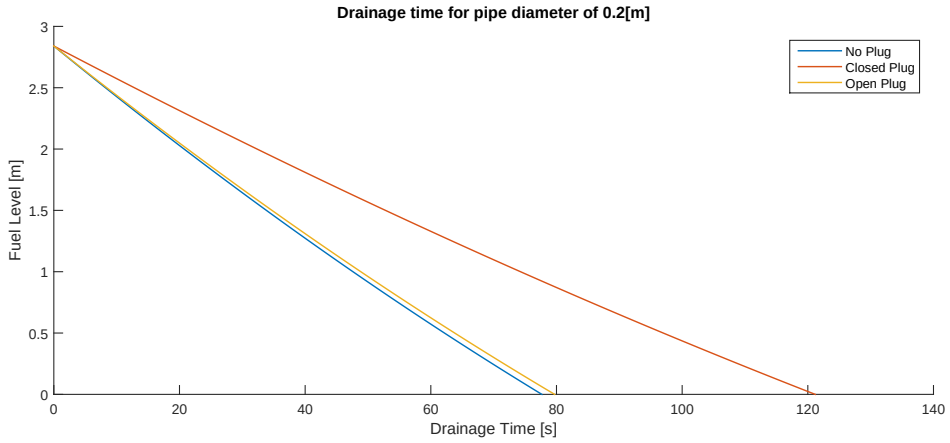

Figure 4.12: Fuel height as a function of time since start of drainage

The drainage times for no plug, open plug and closed plug are 78, 80 and 121 seconds respectively. As expected, the open plug again hardly influences the flow resulting in a nearly equal drainage time compared to no obstruction in the pipe. Note that these calculated times might be an underestimate of the true discharge time because the fluid motion in the tanks is completely ignored. Furthermore, the geometry of the true core and fuel loops are ignored. In the real case scenario, the fluid is not stored in one big cylindrical volume but is distributed over a system of pipes and heat exchangers as well. This will increase the discharging time.

For the next section of this research, we are interested in the flow velocity of the fuel salt in the pipe:

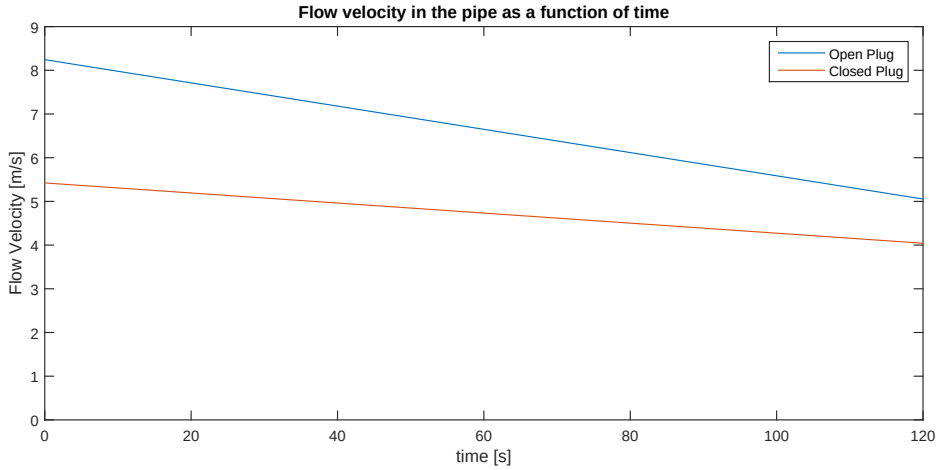

Figure 4.13: Flow velocity of the fluid in the drainage pipe. L_{pipe}=3.5 m

As expected, the flow velocity in the pipe is higher for a non-obstructed flow compared to an obstructed flow. With these results we can check if the assumptions in calculating f are correct. For a velocity of 8.25 m/s Re equals $6.7{\cdot}10^5$, well below 10^6. Furthermore, the velocity domain used for the calculation of f seems to be correct. Next, the influence of the draining tube length and tube radius on the drainage time is explored:

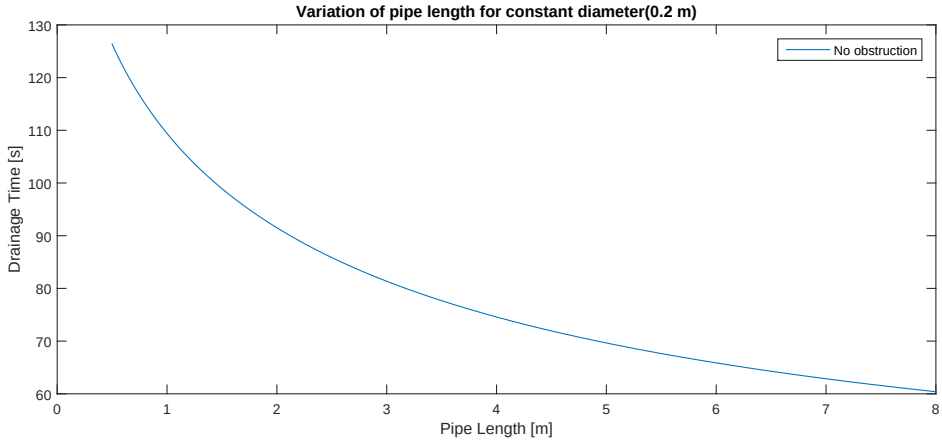

Figure 4.14: Effect of the drainage pipe length on the drainage time

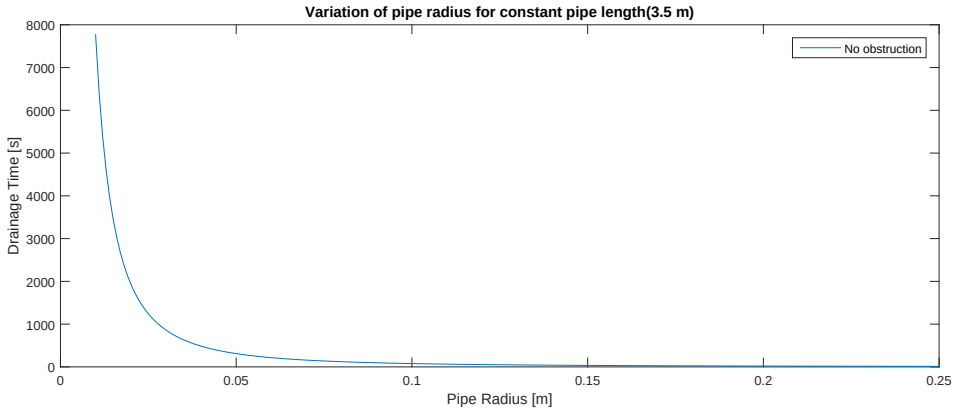

Figure 4.15: Effect of the drainage pipe radius on the drainage time

Figures 4.14 and 4.15 show the expected influence of varying the tube diameter and length. Beyond a radius of 0.1 m the drainage time hardly decreases as the radius increases, this validates the choice for a drainage pipe radius of 0.1 m. From figures 4.14 and 4.15 it is also clear that the pipe diameter has a greater influence on the drainage time compared to the pipe length. Note that for much bigger pipe diameters the solution to the drainage tank problem presented in section 2.1 is invalid since the fluid velocity in the tank will not be negligible.

4.3 Temperature Distribution

This section concerns the CFD in combination with temperature calculations on the fuel salt running through the part of the pipe exposed to the pool below the reactor core. These calculations shed light on the issue if any crystallization of the salt can occur during the draining procedure.

The calculations are conducted on the open plug situation, this translates to a drainage time of 80 seconds with the following time dependent inlet velocity:

$$v(t) = 8.25 - 0.026 \cdot t \tag{4.2}$$

Equation 4.2 corresponds to the blue line depicted in figure 4.13. Note that this equation is valid on the domain t=[0;80] since the reactor is completely drained after 80 seconds. The measurements presented in this section are taken of horizontal and vertical lines in the geometry, these measurement locations are depicted in the following figure.

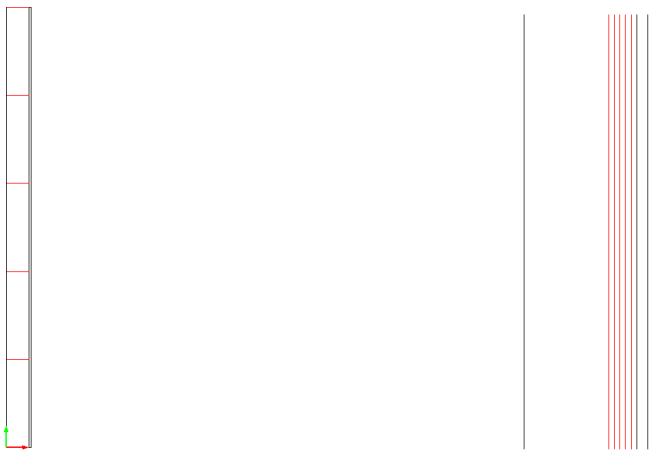

Figure 4.16: Horizontal and vertical lines at which the measurements presented in this section are taken.

Since this model is solved using a time-dependent study, results are available for every 2 seconds of the draining procedure. The results presented in this research are predominantly taken at t=80 s since the velocity will be the lowest and thus cooling of the flow largest. Firstly, results of the development of velocity magnitude throughout the pipe are presented:

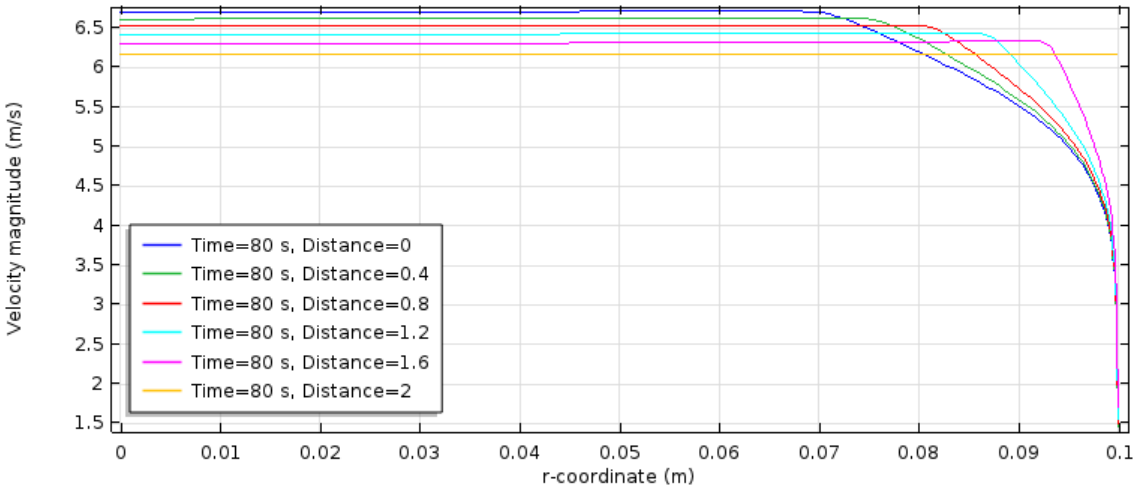

Figure 4.17: Development of the velocity magnitude throughout the pipe. The horizontal axis display the distance from the symmetry axis. Distances [m] displayed are measured in respect to the outlet (z=0) of the pipe.

From figure 4.17 it is clear that the flow front enters the domain straight and quickly develops into a velocity magnitude expected in turbulent flows. However, the flow is still developing since velocity profile still slightly changes downstream. The measurements taken at different time steps (essentially different inlet velocities) look very similar. It is expected that the temperature development behaves similar to velocity magnitude since the heat is, to a certain degree, transferred together with the momentum.

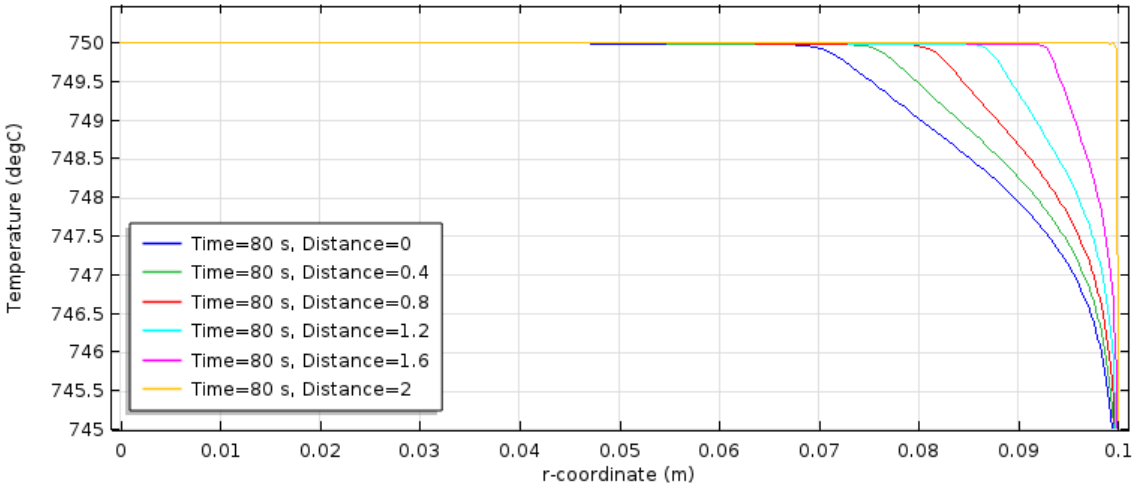

Figure 4.18: Development of the horizontal temperature profile at t=80s. The horizontal axis display the distance from the symmetry axis. Distances [m] displayed are measured from the outlet (z=0) of the pipe.

Figure 4.18 confirms the suspicion that the temperature develops in a similar way to the velocity. However, the temperature is clearly not fully developed since the bulk of the fluid is still 750 °C. Furthermore, only very small drop in temperature observed with temperatures at the wall being only approximately 5 °C lower than the bulk of the flow. To further investigate this, measurements are taken on the vertical lines (see figure 4.16):

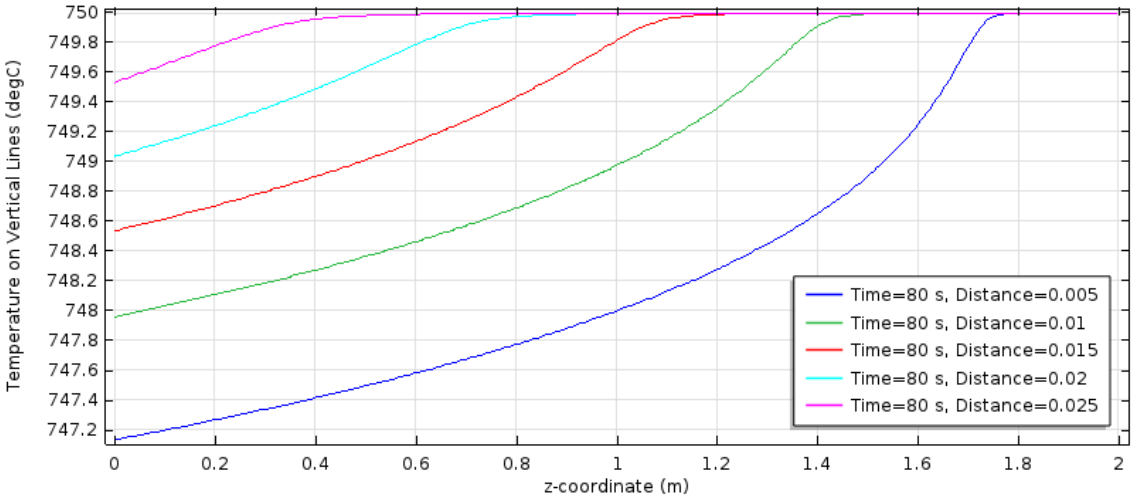

Figure 4.19: Development of the vertical temperature profile at t=80s. The horizontal axis display the distance from the outlet. Distances [m] displayed are measured from the wall.

Figure 4.19 further confirms the small influence of the pool surrounding the pipe on the temperature in the fuel salt flow. Since the fuel salt melts at approximately 565 °C there is no hazard of crystallization in the flow since minimum temperature of the flow seems to be 745 °C. To further investigate this time dependency of the fluid velocity is taken into account.

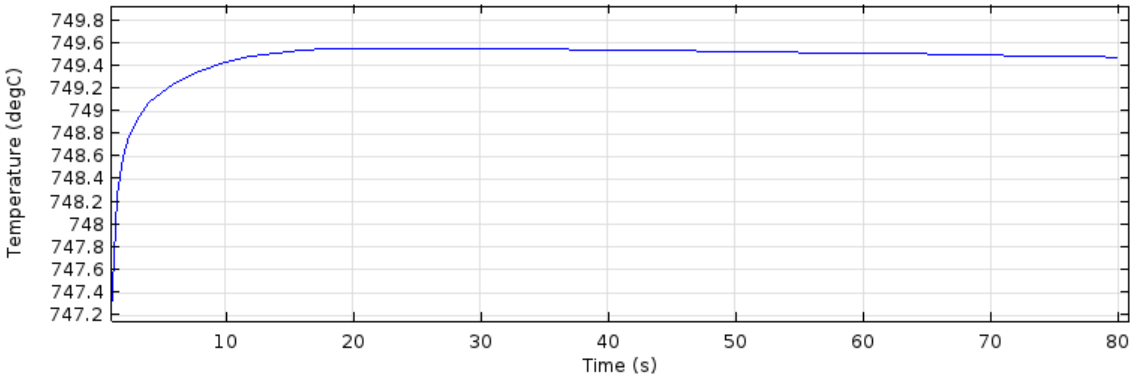

Figure 4.20: Time dependent average fuel salt temperature, measured at the outlet.

In figure 4.20 the time dependence of the average temperature at the outlet is depicted. The average temperature starts out low since initially the wall is 20 °C. As the wall heats up the average temperature of the flow rises to its highest value of 749.5 °C. From there on the temperature drops slowly due to slowing down of the flow.

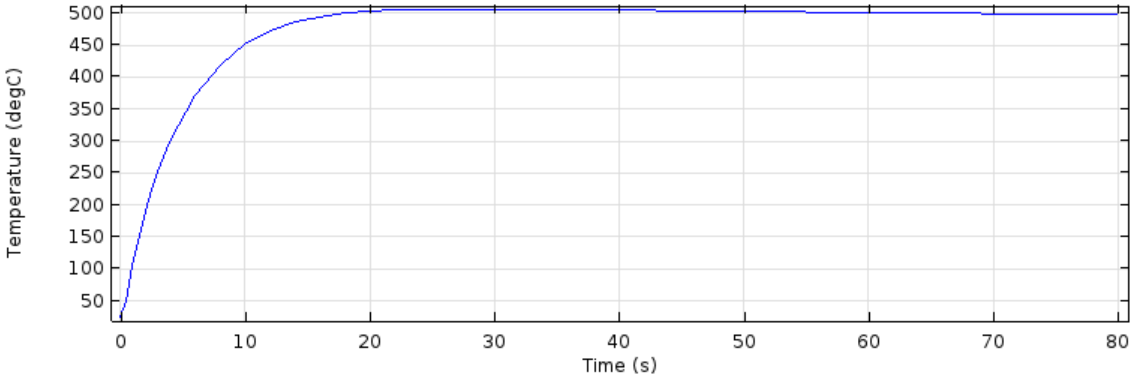

Figure 4.21: Time dependent average wall temperature, measured at the bottom of the wall (z=0).

Figure 4.21 is plotted to confirm the suspicion that the wall heats up as the hot salt flows through the pipe. Within 20 s the wall temperature rises from 20 to 500 °C from where on it stays approximately constant for the entire procedure. Due to this effect the temperature difference between the wall and the salt decreases causing nearly no cooling down of the flow. Further research must consider if Hastelloy-N or any other material can cope with these kind of temperature gradients.

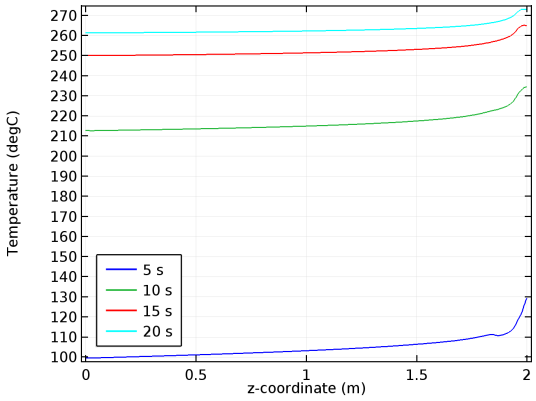

Figure 4.22: Temperature of the outer wall exposed to pool.

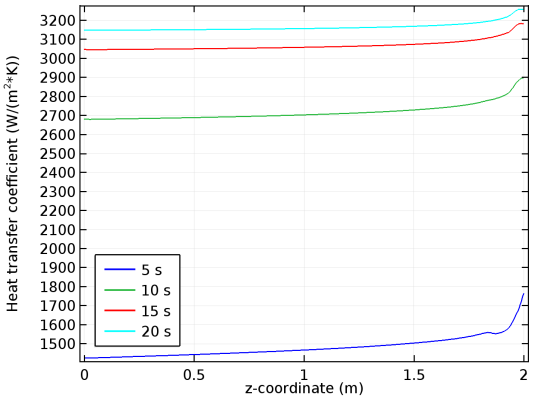

Figure 4.23: Heat transfer coefficient governing the convective heat flux from the pipe to the pool.

The heat is transferred from the pipe to the pool by a convective heat flux, elaborated on in section 2.6. The temperature of the outer wall and the heat transfer coefficient governing the convective heat flux is plotted in figures 4.22 and 4.23. The heat transfer coefficient follows the movements of the wall temperature very closely, this can be explained by the Rayleigh number dependence of the heat transfer coefficient. The Rayleigh number is dependent on the wall temperature and the external temperature. In further research, a comparative study must be done between modelling using a heat transfer coefficient relation and modelling the entire pool. Adding the pool to this model is currently to computational expensive since this would add a flow due to convection in the pool. However, modelling the entire pool will generate more accurate results for the convective heat flux and heat transfer coefficient.

Lastly, a short look is taken at the turbulent thermal conductivity, λ_T, of the fluid:

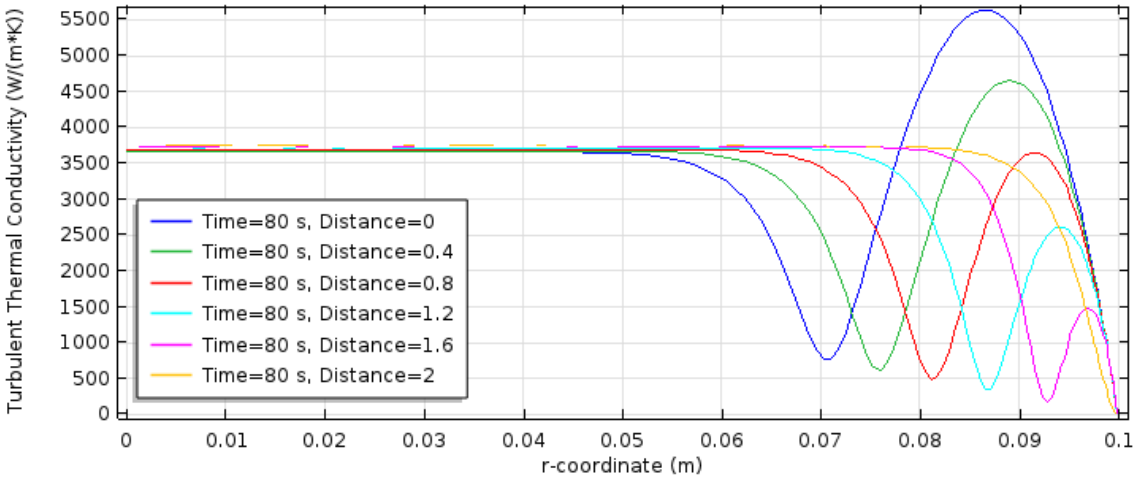

Figure 4.24: Turbulent thermal conductivity in the r-direction of the flow on different distances [m] from the outlet. t=80 s.

The behaviour λ_T is governed by the turbulent Prandtl number and the turbulent viscosity. μ_T exhibits very similar behaviour to λ_T meaning that the turbulent Prandtl number is constant for this flow. In this case $Pr_T = 0.85$. The value for λ_T is multiple times higher than the molecular thermal conductivity λ for the molten salt meaning that, as expected, the turbulent flow significantly increases the thermal conductivity.

The results presented in this last section were derived from the model with the finest mesh (see section 3.4.2). The dimensionless distance to cell centre for this mesh varies between 1.8 and 3, for the different inlet velocities. This is higher than the prescribed value of 0.5. However, a mesh study was conducted by refining the mesh size multiple times. The results calculated with this final mesh were similar to a somewhat coarser mesh, meaning that refinement did not bring any more accurate results. Predicted is that for any more finer mesh sizes the results will not be significantly more accurate. However, further research on this should be conducted.

Chapter 5

Conclusion and Recommendations

Molten Salts Reactors as the MSFR have some characteristics very promising in terms of safety, relying mainly on the possibility to drain the fissile fuel from the reactor. This research aims on investigating the conceptual design of the fuel drainage system. Previous research showed that due to decay heat, the MSFR's fuel salt has to be drained from the reactor within 8 minutes. After 8 minutes the fuel salt reaches temperatures above 750 °C, possibly damaging the reactors components.

In the design under research in this paper a 3.5 m drainage pipe connects the core with the, in a pool submerged, drainage tank below the reactor.The first 1.5 m of drainage pipe runs through the lower reflector and is regarded as insulated. The additional 2 m of pipe runs through the underground pool to the drainage tanks. During normal operation of the MSFR the drainage pipe is closed by a actively cooled freeze plug. In case of a power outage, the freeze plug melts due to the high temperature fuel salt it is contact with.

In order to calculate the drainage time of the MSFR, the resistance coefficient of the plug has te be calculated. Calculations were conducted on a partially melted plug and a completely melted plug using the CFD software Comsol. The resistance coefficients of the partially opened plug equals 2.59 and of the completely opened plug equals 0.19. Using these values and the known measurements of the drainage pipe the MSFR drains in the partially opened situation in 121 seconds and in the completely opened situation in 80 seconds. These calculated drainage times might be an underestimate of the true discharge time because the fluid motion in the reactor is completely ignored, as well as the reactors exact geometry. Furthermore, wall friction due to wall roughness has not been taken into account. However, these values are well below the 8 minutes prescribed and there is no indication that taking the exact geometry of the tank or the friction factor into account will increase the drainage time to more than 8 minutes.

Besides the drainage time and velocity, research was conducted into possible fuel crystallization in the pipe. Crystallization of the salt can block the flow and cause overheating of the system. Using a turbulent non-isothermal flow theory the temperature profile of the fuel is calculated in the last 2 m of the pipe. The results show that no significant cooling of the fuel occurs, when the salt exits the pipe the temperature has only dropped about 1-3°C. Even at the wall temperatures are well above the melting point of the salt meaning that no crystallization will occur. This means the fuel can freely run from the reactor to the underground drainage tanks for safe long term storage.

In this research, the wall thickness of the pipe is set to 1 cm. As the hot salt runs through the piping exposed to the pool, a very steep temperature gradient occurs in the wall material Hastelloy-N. In 20 seconds the average temperature of the wall rises from 20 to 500°C. Further research has to be conducted into the thermal stresses on the wall in order to make sure the walls can cope with these temperature gradients. This includes studies with varying wall thickness and the influence on the temperature distribution.

Furthermore, the problem is split up in two parts: The freeze plug model and the turbulent heat transfer model. For more accurate results these models would have to be combined into one since currently the output flow of the plug model is not the input flow of the heat transfer model. This is done to save computational time. However, adding these two together would generate a more accurate velocity profile. In addition to this, modelling the entire pool surrounding the pipe will result in a more accurate convective heat flux. However, this does add a lot of computational time since the flows through the entire pool have to be calculated for each time step.

In a future research, the actual drainage tanks should be investigated. This involves researching the geometry of the drainage tank or possibly splitting the fuel over multiple smaller drainage tanks. For this research, decay heat has to be taken into account and a system has to be designed to passively transfer the decay heat away from the fuel salt.

Bibliography

K. Abe, T. Kondoh, and Y. Nagano. A new turbulence model for predicting fluid flow and heat transfer in separating and reattaching flows—i. flow field calculations. *International journal of heat and mass transfer*, 37(1):139–151, 1994.

T. L. Bergman, F. P. Incropera, D. P. DeWitt, and A. S. Lavine. *Fundamentals of heat and mass transfer*. John Wiley & Sons, 2006.

R. B. Bird, W. E. Stewart, and E. N. Lightfoot. *Transport Phenomena*. John Wiley & Sons, Inc., New York, second edition, 1960.

M. Brovchenko, D. Heuer, E. Merle-Lucotte, M. Allibert, V. Ghetta, A. Laureau, and P. Rubiolo. Design-related studies for the preliminary safety assessment of the molten salt fast reactor. *Nuclear Science and Engineering*, 175(3):329–339, 2013.

I. B. Celik. Introductory turbulence modeling. Master's thesis, West Virginia University, 1999.

COMSOL. *CFD Module; User's Guide*, 2015.

EVOL. Evol final report, 2013.

W. Frei. Which turbulence model should i choose for my cfd application, 2013. URL `https://www.comsol.com/blogs/which-turbulence-model-should-choose-cfd-application/`.

D. Heuer, E. Merle-Lucotte, M. Allibert, M. Brovchenko, V. Ghetta, and P. Rubiolo. Towards the thorium fuel cycle with molten salt fast reactors. *Annals of Nuclear Energy*, 64:421–429, 2014.

S. Hulshoff. *CFD II Part 2: Computation and Modelling of Turbulence*. TU Delft, 2015.

L. Janssen and M. Warmoeskerken. *Transport Phenomena Data Companion*. VSSD, Delft, third edition, 1987.

W. M. Kays. Turbulent prandtl number—where are we? *Journal of Heat Transfer*, 116(2):284–295, 1994.

I. Koks. Melting behaviour of the freeze plug in a molten salt fast reactor, 2016.

E. Merle-Lucotte, M. Allibert, D. Heuer, M. Brovchenko, A. Laureau, V. Ghetta, and P. Rubiolo. Preliminary design studies of the draining tanks for the molten salt fast reactor. In *European Nuclear Conference (ENC 2014)*, pages 220–230, 2014.

F. A. Morrison. Data correlation for friction factor in smooth pipes, 2013. URL `http://www.chem.mtu.edu/ fmorriso/DataCorrelationForSmoothPipes2013.pdf`.

H. van den Akker and R. Mudde. *Fysische transportverschijnselen*. Delft Academic Press, Delft, fourth edition, 1996.

S. Wang, M. Massone, and A. Rineiski. Analytical investigation of the draining system for a molten salt fast reactor. 2016.

B. Weigand, J. Ferguson, and M. Crawford. An extended kays and crawford turbulent prandtl number model. *International journal of heat and mass transfer*, 40(17):4191–4196, 1997.

D. C. Wilcox et al. *Turbulence modeling for CFD*, volume 2. DCW industries La Canada, CA, 1998.

Appendices

Matlab Code Resistance Coefficient

Closed Plug

```
v= [2:0.5:6.5];
deltaP=[18552
30256
44757
62011
81974
1.0468E5
1.3005E5
1.5802E5
1.8888E5
2.2261E5];
rho=4125;
g=9.81;
h=1.435;
y=2*(deltaP./rho);
v2=v.^2;

x=v.';
x2=v2.';
p = polyfit(x2,y,1)

hold on
figure(1)
plot(v,y,'-o')
title('Pressure differce against Inlet velocity for Closed Plug')
xlabel('Inlet Velocity [m/s]')
ylabel('2 \Delta p/\rho [J/kg]')
hold off

hold on
figure(2)
plot(v2,y,'-o')
title('Pressure differce against the square of the Inlet velocity for Closed Plug')
xlabel('Inlet Velocity Squared [m^2/s^2]')
ylabel('2 \Delta p/\rho [J/kg]')
hold off
```

Open Plug

```
vb= [2:0.5:6.5];
deltaP=[1876.3
2839.0
3980.1
5297.1
6787.4
8446.0
10269
12254
14396
16694
];
rho=4125;
g=9.81;
h=1.435;
yb=2*(deltaP./rho);
vb2=vb.^2;

xb2=vb2.';
p = polyfit(xb2,yb,1)

hold on
figure(1)
plot(vb,yb,'-o')
title('Pressure differce against Inlet velocity for Open Plug')
xlabel('Inlet Velocity [m/s]')
ylabel('2 \Delta p/\rho [J/kg]')
hold off

hold on
figure(2)
plot(vb2,yb,'-o')
title('Pressure differce against the square of the Inlet velocity for Open Plug')
xlabel('Inlet Velocity Squared [m^2/s^2]')
ylabel('2 \Delta p/\rho [J/kg]')
hold off
```

Matlab Code Drainage Time

```
clear all; close all; clc

H=2.84;
r=1.42;
rho=4080;
mu=1.01*10^-2;
g=9.81;
dt=0.01;
t=0:dt:180;
R=0.1;
f= 0.0034;
D=2*R;

%%
Ktot= 0.5;
```

```
L_niks=3.5;

k=sqrt(2*g/(1+4*f*(L_niks/D)+Ktot))*(R/r)^2;
h=0.25*k^2*t.^2-sqrt(H+L_niks)*k*t+H;


%% Closed Plug
KClosed= 0.5 + 2.59;
L=2.065;
L2=3.5;
k_closed=sqrt(2*g/(1+4*f*(L/D)+KClosed))*(R/r)^2;
h_closed=0.25*k_closed^2*t.^2-sqrt(H+L2)*k_closed*t+H;

%% Open Plug
KOpen= 0.5 + 0.19;
L=2.065;
L2=3.5;
k_open=sqrt(2*g/(1+4*f*(L/D)+KOpen))*(R/r)^2;
h_open=0.25*k_open^2*t.^2-sqrt(H+L2)*k_open*t+H;

figure(1)
hold on
axis([0 140 0 3])
plot(t,h,'LineWidth',1)
plot(t,h_closed,'LineWidth',1)
plot(t,h_open,'LineWidth',1)
ylabel('Fuel Level [m]')
xlabel('Drainage Time [s]')
title('Drainage time for pipe diameter of 0.2[m]')
legend('No Plug','Closed Plug','Open Plug')
hold off


%%

v_open=sqrt(2*g*(h_open+L2)/(1+4*f*(L/D)+KOpen));
v_closed=sqrt(2*g*(h_closed+L2)/(1+4*f*(L/D)+KClosed));
phi_m=pi*R*R*rho*v_open;
figure(2)
plot(t,phi_m)
xlabel('time')
ylabel('Mass Flow [kg/s]')
figure(3)
plot(t,v_open,t,v_closed)
axis([0 120 0 9])
xlabel('time [s]')
ylabel('Flow Velocity [m/s]')
legend('Open Plug','Closed Plug')
title('Flow velocity in the pipe as a function of time')
polyfit(t,phi_m,1);
polyfit(t,v_open,1)
polyfit(t,v_closed,1);

%%
rho=4080;
visc=1.01*10^-2;
```

```
d=0.2;
g=9.81;
vv=[4.5:0.1:7];
Re=(rho*vv*d/visc);
f=16./Re + (0.0076*(3170./Re).^0.165)./(1+(3170./Re).^7);
y=4*f;
B=0.316*Re.^-0.25;
figure(4)
plot(vv,f,'-')
xlabel('Velocity [m/s]')
ylabel('Fanning Friction Factor')
title('f as a function of velocity')

%%
K=0.5;
g=9.81;
L=3.5;
f=0.0034;
r=1.42;
R=0.1;
H=2.84;
t_niks=(r/R)^2*sqrt(2*(4*f*(L/D) + K + 1)/(g))*(sqrt(H+L)-sqrt(L))

%%
K=0.5+0.19;
L2=2.065;
t_open=(r/R)^2*sqrt(2*(4*f*(L2/D) + K + 1)/(g))*(sqrt(H+L)-sqrt(L))

%%
K=0.5+2.59;
t_closed=(r/R)^2*sqrt(2*(4*f*(L2/D) + K + 1)/(g))*(sqrt(H+L)-sqrt(L))

%%
K=0.5;
g=9.81;
f=0.0034;
r=1.42;
R=0.1;
H=2.84;
L=[0.5:0.01:8];
D=2*R;
t_eff=(r/R)^2*sqrt(2*(L.*4*f/D + K + 1)/(g)).*(sqrt(H+L)-sqrt(L));
plot(L,t_eff)
xlabel('Pipe Length [m]')
ylabel('Drainage Time [s]')
title('Variation of pipe length for constant diameter(0.2 m)')
legend('No obstruction')
```